Dynamic performance simulation and control of gas turbines used for hybrid gas/wind energy applications

Tsoutsanis, Elias; Meskin, Nader

DOI:
10.1016/j.applthermaleng.2018.09.031

Document Version
Peer reviewed version

Citation for published version (Harvard):
Tsoutsanis, E & Meskin, N 2019, 'Dynamic performance simulation and control of gas turbines used for hybrid gas/wind energy applications', *Applied Thermal Engineering*, vol. 147, pp. 122-142. https://doi.org/10.1016/j.applthermaleng.2018.09.031

Dynamic performance simulation and control of gas turbines used for hybrid gas/wind energy applications

Elias Tsoutsanis[a,*], Nader Meskin[b]

[a] *Department of Mechanical Engineering, University of Birmingham, Birmingham, UK*
[b] *Department of Electrical Engineering, College of Engineering, Qatar University, Doha, Qatar*

Abstract

The exponential growth of renewable electricity generation has transformed significantly the operating environment of gas turbines. Nowadays, gas turbines operate under transient conditions to support their renewable partners. Gas turbine dynamic performance simulation provides the means for assessing the engine behavior and designing engine controllers that will enable them to fulfill their new operating role.

This paper presents a novel gas turbine performance system for representing the nonlinear behavior of a two-shaft gas turbine engine. The developed gas turbine engine model in MATLAB/Simulink environment is capable of simulating both steady state and transient operating conditions, and to facilitate the design of controllers for stable engine operation. Validation of the developed engine model with a gas turbine simulation package confirmed the excellent agreement among all the simulated measurements at transient conditions. The simulated behavior of a hybrid gas/wind power plant enabled the development of an optimized controller for empowering the gas turbine to support the intermittent wind turbines. The time responses of the main parameters of the hybrid gas/wind power plant demonstrated the significant amount of transient conditions that a gas turbine experiences for fulfilling the energy gap imposed by the wind turbines. Finally, the performance comparison of the hybrid power plant to a twin gas turbine power plant highlighted the effective reduction in NO_x emissions.

Keywords: Gas Turbine Performance, MATLAB/Simulink, Engine Control, Transient Performance, Hybrid Power Plant

Highlights

- An engine model for predicting the steady state and transient performance of a gas turbine is presented.
- The model is developed in the object-oriented MATLAB/Simulink environment and validated towards a gas turbine simulation software package.

*Corresponding author
Email address: i.tsoutsanis@bham.ac.uk (Elias Tsoutsanis)

- The observed model behavior aided the development of a controller for regulating engine fuel flow.
- The analysis of a hybrid gas/wind power plant enabled the optimization of the gas turbine operation.
- The hybrid plant demonstrated a significant reduction of NO_x emissions compared to a twin gas turbine power plant.

1. Introduction

The exploitation of renewable energy sources towards a sustainable energy environment has affected the operating profile of the fossil-fueled dominating gas turbines. The intermittent nature of renewables prompts the gas turbines to operate with increased flexibility, for supporting their renewable plant partners and maintaining the stability of the electricity grid [1, 2]. Fast start up, shut down, load following modes, and part load operation [3, 4, 5] are dominating the operating regime of today's gas turbines. Understanding the behavior of these engines, under such demanding operating conditions, is crucial for their successful operation and maintenance (O&M). For the above purpose, engine manufacturers invest a vast amount of their resources and human capital exclusively for modeling, monitoring, and analyzing the performance of power plants [6]. An example of this digital transformation can be found in the Predix technology [7] developed by GE which provides numerous analytic capabilities for power plants. In the near future, O&M of gas turbines is going to be dominated by the application of such technologies as it is evident from the recent integration of GE's Predix to Apple's iPads and iPhones for enabling users to monitor industrial equipment from their personal devices [8].

Gas turbine engine models have a pivotal role in this digital platform, since their simulations aid the development of engine controllers [9, 10] and the optimization of operating schedules. Traditionally, the studies of industrial gas turbine operations have focused on their steady state behavior, with little attention paid to the transient operation. However, a significant portion of the daily energy demand from industrial gas turbines, in today's diverse and intermittent energy mix, involves transient conditions. Consequently, studies that explore the dynamic simulation aspect of gas turbines [11, 12, 13] have recently gained considerable attention.

The reason for this shift lies in the fact that dynamic engine models are capable of assessing the behavior of an engine for a wide range of operating conditions including transient operation [14]. In addition, dynamic models enable novel diagnostics [15, 16, 17] and prognostics solutions [18, 19] which indeed improve the O&M of gas turbines. Therefore, the recently transformed gas turbine operating profile has motivated the development of robust, modular, flexible, and accurate engine models that can facilitate the performance analysis of gas turbines in real-time conditions. Moreover, the observed engine model behavior at transient operating conditions has the potential to aid the design of engine controllers that will enable modern gas turbines to fulfill their role in this dynamic and flexible operating environment

Numerous approaches of variable fidelity have been developed for simulating the gas turbine behavior [20, 21, 22, 23, 24]. The most commonly used simulation approach, that enables real-time condition monitoring and diagnosis, is the zero dimensional (0-D) modeling approach [25], that provides a fast and accurate assessment of the engine behavior at both steady and dynamic conditions. The dynamic performance of the engine is characterized by its state change, due to the regulation of fuel and under these conditions the aim of the simulation is to identify key performance trends that might lead to phenomena such as compressor surge and/or violation of the turbine entry temperature (TET) limits of engine. The performance simulation of the engine can provide invaluable insights of its behavior, and especially for cases where experimental tests are not feasible to be carried out and might prove catastrophic for the engine, as described by [26].

The two fundamental approaches for dynamic engine simulation are the iterative constant mass flow (CMF) method [27, 28, 29, 30] and the inter-component volume (ICV) method [31]. Both of these methods have been extensively used for performance simulation studies of gas turbines [32, 33, 34]. The ICV method [35] assumes that during transient operations there are mass flow imbalances. The CMF method [36] is an iterative process initiated by guessed engine component parameters such as pressure ratio and then an engine model run is carried out. Then the observed errors in the simulated mass flow rates are progressively minimized by modifying the initial guessed values of the parameters by the Newton-Raphson iterative approach.

In this paper, a gas turbine engine model of a two-shaft gas turbine is developed in MATLAB/Simulink environment. In contrary to other simulation packages for gas turbines, MATLAB/Simulink environment facilitates the design of controllers, and injection of degradation signals into the engine model components and/or sensors for diagnostic and prognostic studies. Therefore, numerous engine degradation scenarios [37, 38, 39] can be simulated and the outcome of this process is a good quality dataset for testing diagnostic and prognostic algorithms. The developed engine model combines the above two approaches, since the CMF iterative method [40, 41] used for steady state is subsequently integrated with the ICV method for transient performance simulation.

The initialization phase of a dynamic engine model is of crucial importance, as it refers to the steady state iterative component matching computation. If this process is not properly integrated into the dynamic engine model it leads to an initial oscillating engine response, before it stabilizes to a steady state condition, that is also contributing to the subsequent transient maneuvers of the engine. The majority of the previous works for the steady state conditions of an engine, rely on the assumption that the fuel flow entering the combustion chamber is negligible in comparison to the air mass flow rate. This assumption is transferable to the flow and work compatibilities, where the additional fuel flow is commonly ignored, and determined after the matching process. Although this is a typical practice for gas turbine performance analysis, it causes initialization problems when the same engine model architecture is used for transient studies, where the fuel flow rate is the control input.

To address this common issue of engine transient modeling, the authors propose the integration of steady state component matching process in the initial state of the dynamic engine model [42]. Therefore, the inclusion of an additional fuel flow iteration in the CMF method allows the accurate establishment of the initial state of the engine model, which subsequently implements the faster ICV method for transient conditions. The dynamic engine model implements a family of component performance maps, as look up tables, and is represented by a set of first order differential equations, which are added to the steady state thermodynamic equations. The transient performance simulations highlighted some key issues that might be hazardous for a real engine. This prompted the development of an engine controller for enabling smooth and safe engine operation. The engine model is validated towards PROOSIS [43] gas turbine simulation software. Time responses of several engine model variables are compared with the PROOSIS simulated results.

Moreover, the engine model behavior is assessed when the gas turbine is working in partnership with a wind farm in a hybrid gas/wind power plant. A family of wind turbines has been used from MATLAB/Simulink environment and coupled with the developed gas turbine model. Under fluctuating energy demand and variable wind speed, the gas turbine is stressed to operate under fast transient conditions. This simulated study gives additional insights of the engine dynamic behavior that has the potential to serve as a useful guide for designing and optimizing of engine controllers suitable for hybrid power plants operation. Finally, the performance of the hybrid power plant has been compared to a twin gas turbine power plant for assessing the shutdown capability of the gas turbines and their corresponding NO_x emissions.

To summarize, the major contributions of this work are as follows:

- An engine model representing a two-shaft industrial gas turbine has been developed in MATLAB/Simulink environment. The engine model consists of component characteristic maps and their corresponding governing thermodynamic equations.
- At steady state conditions, the engine model satisfies mass flow, work, and speed compatibilities through an iterative procedure. Moreover, an additional iterative process is integrated into the engine model for determining the fuel flow rate.
- The transient engine model has been developed based on the ICV method. The initialization of the transient engine model parameters, which is of crucial importance for the generic behavior of the engine at dynamic operating conditions, has been achieved by its steady state counterpart. Initial values for the fuel flow rate, pressures, and shaft rotational speed are given by the steady state model.
- The observations from the simulated behavior of the engine model, at transient operating conditions, enabled the development of a controller which optimizes the fuel flow injected into the engine for maintaining a safe and reliable operation.

- The engine model has been validated towards a well-established gas turbine simulations package called PROOSIS.
- The developed gas turbine model has been coupled to a wind turbine model in MATLAB/Simulink and the dynamic performance of the gas turbine is assessed for meeting the fluctuating energy demand while the wind speed varies with respect to time.
- The hybrid power plant has been also compared to a twin gas turbine power plant in order to evaluate the NO_x emissions by implementing an emissions prediction model available from the literature [44].
- To the authors best knowledge, this is the first time in the literature that the iterative steady-state approach has been fully integrated into a dynamic engine model developed in MATLAB/Simulink environment, and subsequently tested for designing and optimizing engine controllers for hybrid gas/wind power plants.

The remainder of this paper is organized as follows. In Sec. 2, the methodology employed for the steady state and transient performance simulation along with the controller design and the validation approach are described. The results of the Case Studies are presented and discussed in Sec. 3, followed by the conclusions in Sec. 4.

2. Methodology

2.1. Gas Turbine Mathematical Model

For this study, an engine model of a two-shaft industrial gas turbine is developed in MATLAB/Simulink. The system consists of a gas generator and a free power turbine. The main components of the gas generator are the compressor, combustor, and turbine. The exhaust gases of the gas generator are driving the power turbine which is coupled to an electricity generator as seen from Fig. 1.

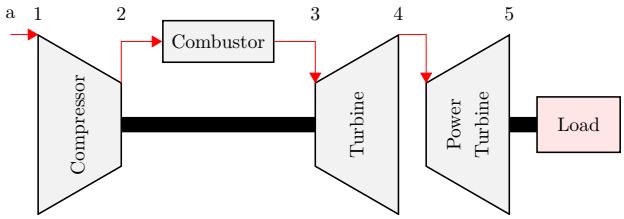

Figure 1: Representation of the two-shaft engine model along with its station numbering.

The thermodynamic performance simulation of each engine component is described in the following subsections. The following notation is used throughout the paper. Temperatures and pressures are denoted by T_i and P_i, respectively where subscript $i = a, 1, 2, 3, 4, 5$ represents the engine station.

2.1.1. Compressor

It should be noted that it is a common practice for performance analysis studies of industrial gas turbines to ignore the inlet losses and assume that the inlet is ideal. This means that $P_a = P_1$, and $T_a = T_1$. The compressor performance is often represented by a characteristic map which presents the interrelationships between pressure ratio $\pi_c = P_2/P_1$, isentropic efficiency η_c, corrected mass flow $\dot{m}_1\sqrt{T}_1/P_1$, and corrected shaft rotational speed $N/\sqrt{T}_1$, as seen from Figs. 2 and 3. Scaled maps from PROOSIS [43] simulation software have been used in this model.

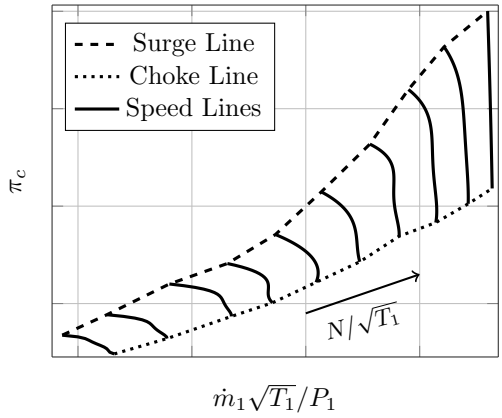

Figure 2: Compressor performance map for $\dot{m}_1\sqrt{T}_1/P_1$ vs π_c relationship.

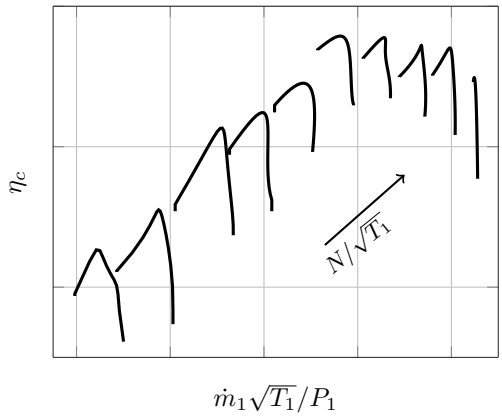

Figure 3: Compressor performance map for $\dot{m}_1\sqrt{T}_1/P_1$ vs η_c relationship.

Once the outputs of the map are determined, the temperature rise ΔT_{12} across the compressor is computed as follows:

$$\Delta T_{12} = \frac{T_1}{\eta_c}\left[\left(\frac{P_2}{P_1}\right)^{\frac{\gamma_a-1}{\gamma_a}} - 1\right] \tag{1}$$

The work required to drive the compressor is given by

$$W_c = \dot{m}_1 \cdot c_{p_a} \cdot \Delta T_{12} \tag{2}$$

where c_{p_a} denotes the specific heat of air.

2.1.2. Combustor

The energy balance equation is governing the performance of the combustor as follows:

$$\dot{m}_1 \cdot c_{p_a} \cdot T_2 + \dot{m}_f \cdot LHV = \dot{m}_3 \cdot c_{p_g} \cdot T_3 \tag{3}$$

where LHV denotes the low heat value of fossil fuel used, and c_{p_g} denotes the specific heat of combustion products. The heat input HI to the system is given by the following equation:

$$HI = \dot{m}_f \cdot LHV \tag{4}$$

which is subsequently used for determining thermal efficiency η_{th}.

Combustor flame-out or flame instabilities could be addressed by high fidelity Direct Numerical Simulations (DNS), Large Eddy Simulations (LES) and Reynolds Average Navier-Stokes Simulations (RANS), once the combustor specifications are known [45]. The integration of such numerical simulations into real-time 0-D gas turbine models is not only computationally expensive but also beyond the focus of this study, which is the development of a reliable, accurate and computational efficient dynamic model that can be potentially used for condition monitoring purposes. However, a simple approach could be adopted for establishing the engine's limitations for fast transient maneuvers. Description of the above process is discussed in Case Study 2 in the Results Section.

In terms of emissions, the nitrogen oxides prediction model for gas turbines developed by Rokke et al. [46] and verified by Pires et al. [44], for engines ranging in power from 1.5 MW to 34 MW, is implemented in this model. The equation used for determining the NO_x emissions is given by:

$$NO_x = 18.1 \cdot (P_2/P_1)^{1.42} \cdot \dot{m}_1^{0.3} \cdot f^{0.72} \tag{5}$$

where P_2/P_1 denotes compressor pressure ratio, $\dot{m}_1$ denotes air mass flow rate, and f denotes fuel to air ratio (i.e. $\dot{m}_f/\dot{m}_1$). The NO_x emissions are measured in ppmv (parts per million by volume) at 15% O_2.

2.1.3. Turbine

Similar to the compressor, turbine performance is represented by a set of characteristic maps that present the interrelationships between turbine pressure ratio π_t, corrected mass flow $\dot{m}_3\sqrt{T_3}/P_3$, efficiency η_t, and corrected rotational speed $N/\sqrt{T_3}$, as seen from Figs. 4 and 5.

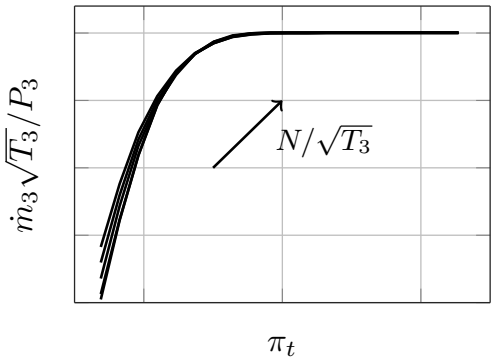

Figure 4: Turbine performance map for π_t vs $\dot{m}_3\sqrt{T_3}/P_3$ relationship.

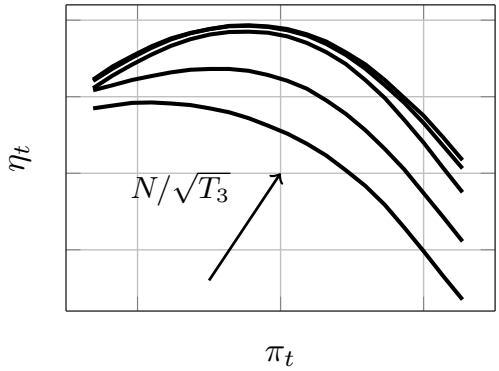

Figure 5: Turbine performance map for π_t vs η_t relationship.

It follows that the temperature drop ΔT_{34} across the turbine is computed by:

$$\Delta T_{34} = \eta_t \cdot T_3 \left[1 - \left(\frac{1}{\pi_t} \right)^{\frac{\gamma_g - 1}{\gamma_g}} \right] \tag{6}$$

where γ_g is the heat capacity ratio of combustion products and for preliminary performance calculations it may be assumed constant, i.e. $\gamma_g = 1.33$. The work extracted by the turbine is given by:

$$W_t = \eta_m \cdot \dot{m}_3 \cdot c_{p_g} \cdot \Delta T_{34} \tag{7}$$

where c_{p_g} denotes the specific heat of combustion gases and η_m denotes the mechanical efficiency.

2.1.4. Power Turbine

Similar to the turbine, free power turbine performance is represented by characteristic maps that present the interrelationship between power turbine pressure ratio π_{pt}, corrected mass flow $\dot{m}_4\sqrt{T_4}/P_4$, efficiency η_{pt}, and corrected rotational speed $N_{pt}/\sqrt{T_4}$, as seen from Figs. 6 and 7.

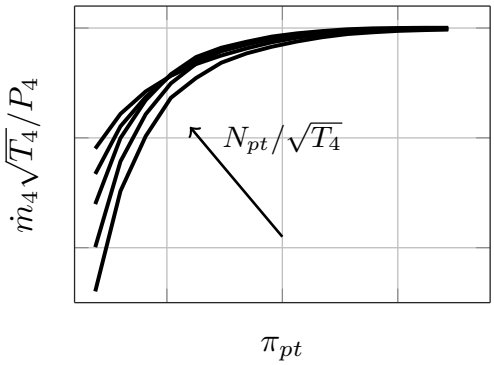

Figure 6: Power turbine performance map for π_{pt} vs $\dot{m}_4\sqrt{T}_4/P_4$ relationship.

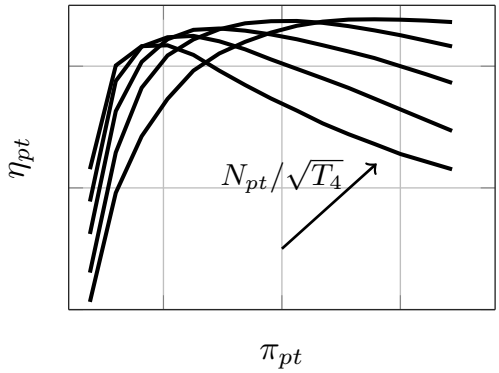

Figure 7: Power turbine performance map for π_{pt} vs η_{pt} relationship.

194 The temperature drop ΔT_{45} across the power turbine is given by:

$$\Delta T_{45} = \eta_{pt} \cdot T_4 \left[1 - \left(\frac{1}{\pi_{pt}} \right)^{\frac{\gamma_g - 1}{\gamma_g}} \right] \tag{8}$$

195 For this study, the power turbine is coupled to a generator for producing electricity, so its speed will be
196 assumed constant. The work extracted by the power turbine is the useful work UW of the gas turbine and
197 is given by

$$UW = \dot{m}_4 \cdot c_{p_g} \cdot \Delta T_{45} \tag{9}$$

198 The thermal efficiency of the gas turbine system is given by:

$$\eta_{th} = 100 \cdot \frac{UW}{HI} \tag{10}$$

199 and expressed as a percentage. It is important at this point to describe the gas turbine engine simulation
200 process.

2.2. Steady State Simulation

2.2.1. Assumptions

To make the steady state performance model generic and easy to implement, the following assumptions have been made:

1. Inlet and exhaust pressure losses are ignored (i.e. $P_a = P_1$, $T_a = T_1$, and $P_5 = P_a$).
2. The fuel flow rate $\dot{m}_f$ is not considered negligible, in comparison to the air mass flow rate $\dot{m}_1$, so it has been included in the flow and work compatibility equations.
3. As shown in Fig. 4, the variation of $N/\sqrt{T_3}$ is negligible in the turbine map of π_t vs $\dot{m}_3\sqrt{T_3}/P_3$ relationship, so this map has been simplified to one which presents a single curve of $N/\sqrt{T_3}$.
4. The geometry of the compressor is fixed.
5. There is no turbine cooling consideration.

The above assumptions rely on the fact that the focus of this study is to examine the behavior of a gas turbine system that may be used as a benchmark model for designing controllers, simulating degradation scenarios and testing diagnostic and prognostic solutions. Since the model-based control, diagnostic and prognostic studies are based on the measurement Δs (i.e. the measurement differences) this means that a robust and dynamic engine model will suffice for the above purposes. However, if one wants to take into consideration additional parameters such as compressor variable geometry, variable stator vanes (VSV) scheduling, and turbine cooling to name a few, then the developed model is modular enough to accommodate these additions.

2.2.2. Simulation Process

The analysis carried out here is focusing on establishing the engine performance at steady state conditions for a wide range of shaft rotational speeds. Parameters that have to be guessed for this iterative procedure are compressor pressure ratio π_c, turbine pressure ratio π_t, and fuel flow rate $\dot{m}_f$.

The following equations are used to determine the key performance parameters of the gas generator. The *flow compatibility* between compressor and turbine is given by:

$$\frac{\dot{m}_3\sqrt{T_3}}{P_3} = \frac{\dot{m}_1\sqrt{T_1}}{P_1} \cdot \frac{P_1}{P_2} \cdot \frac{P_2}{P_3} \cdot \sqrt{\left(\frac{T_3}{T_1}\right)_F} \cdot \frac{\dot{m}_3}{\dot{m}_1} \tag{11}$$

and allows the determination of $(T_3/T_1)_F$ which denotes the temperature ratio obtained by flow compatibility. The *work compatibility* between compressor and turbine is expressed as follows:

$$\frac{\Delta T_{34}}{T_3} = \frac{\Delta T_{12}}{T_1} \cdot \left(\frac{T_1}{T_3}\right)_W \cdot \frac{c_{p_a}}{c_{p_g}} \cdot \frac{\dot{m}_1}{\dot{m}_3} \tag{12}$$

and used for the computation of another value of $(T_3/T_1)_W$ denoting the temperature ratio obtained from work compatibility. It should be noted that the fuel flow has been included in both Eqs. (11) and (12) where $\dot{m}_3 = \dot{m}_1 + \dot{m}_f$.

The *speed compatibility* is implemented for determining the corrected shaft rotational speed of the gas generator turbine $N/\sqrt{T_3}$ as follows:

$$\frac{N}{\sqrt{T_3}} = \frac{N}{\sqrt{T_1}} \cdot \sqrt{\left(\frac{T_1}{T_3}\right)_F} \tag{13}$$

Finally, the *flow compatibility* between the two turbines is given by:

$$\left(\frac{\dot{m}_4\sqrt{T_4}}{P_4}\right)_F = \frac{\dot{m}_3\sqrt{T_3}}{P_3} \cdot \frac{P_3}{P_4} \cdot \sqrt{\frac{T_4}{T_3}} \tag{14}$$

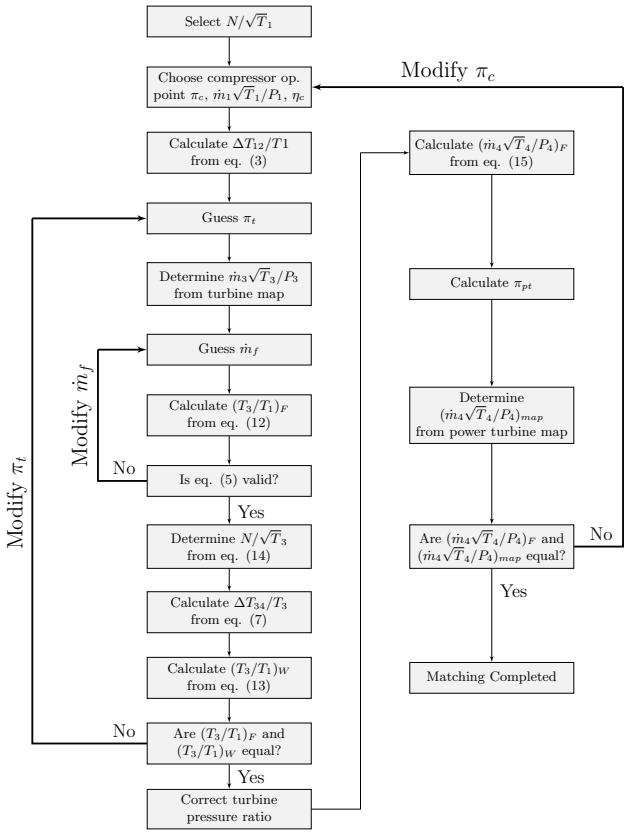

Figure 8: Flow chart of the engine model simulation process at steady state conditions.

The simulation process and the computational interaction among the engine components are schematically represented in Figs. 8 and 9, respectively. The engine model has been developed in the Simulink environment. Simulink is a popular simulation platform that allows the application of numerical analysis methods and has also the potential of implementing the behavior of a system for designing controllers

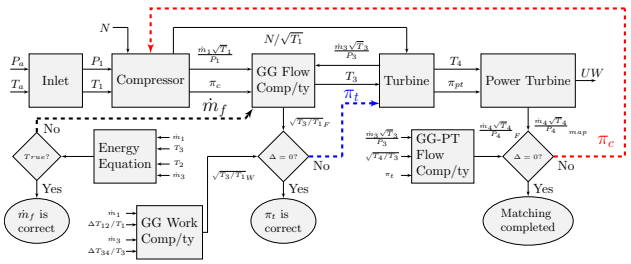

Figure 9: Schematic representation of the modular computational interactions of the steady state engine model. Note that GG:Gas Generator; PT:Power Turbine; Comp/ty:Compatibility.

[47, 48]. The model consists of a set of subsystems for simulating the components of the gas turbine and their thermodynamic interrelationships. The steady state simulation is not only useful for examining the off-design behavior of the gas turbine but more importantly for facilitating the initialization of the dynamic model, a process that affects significantly the accuracy of the transient operational envelope.

For the steady state model, π_c, $\dot{m}_f$, and π_t have to be initially guessed for the iterative computation procedure. The initially guessed parameters corresponding to the design point performance of the engine are summarized in Table 1.

Table 1: The values of the initial guessed parameters for the steady state engine model.

Symbol	Parameter	Value	Units
$\dot{m}_f$	fuel flow rate	1.68	kg/s
π_c	compressor pressure ratio	14.57	-
π_t	turbine pressure ratio	3.62	-

Three algebraic constraints are implemented in Simulink for guessing $\dot{m}_f$, π_t, and π_c in order to satisfy the above. The built-in algebraic constraint block of Simulink, as shown in Fig. 10, has the capability to constrain the input signal $f(x)$ to 0 and outputs an algebraic state x. In order for the algebraic constraint to work, the output x must affect the input $f(x)$ through a direct feedback path.

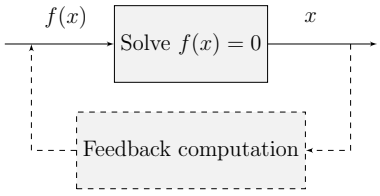

Figure 10: Schematic representation of the algebraic constraint used in Simulink.

For instance, at the final step of the simulation procedure the two values of corrected mass flow rates

of the power turbine available from the map $(\dot{m}_4\sqrt{T_4}/P_4)_{map}$ and the flow compatibility $(\dot{m}_4\sqrt{T_4}/P_4)_F$ are compared. Their difference $\Delta(\dot{m}_4\sqrt{T_4}/P_4)$ is the input signal $f(x)$ to the algebraic constraint. If the two values are not the same (i.e.$f(x) \neq 0$), then a new value of compressor pressure ratio π_c has to be selected. The selected π_c is essentially the output of this algebraic constraint x. This algebraic constraint works because it satisfies the condition in which the selection of π_c affects the feedback computation of their difference, which acts as the input to this block, i.e. $f(\pi_c) = \Delta(\dot{m}_4\sqrt{T_4}/P_4)$.

2.3. Transient Simulation

For the transient performance analysis, a dynamic engine model has been developed in Simulink based on the ICV method. The ICV method assumes the existence of mass flow imbalances during the dynamic operation. For implementing this method, two plenum volumes are integrated in the engine model, as seen from Fig. 11. The characteristic maps used in this dynamic model are the same with its steady state counterpart.

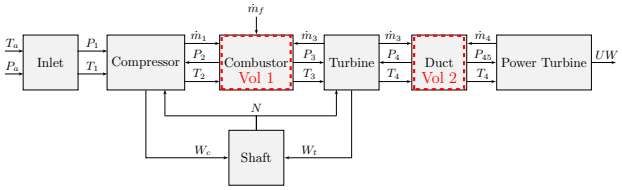

Figure 11: Schematic representation of the modular computational interaction of the transient engine model.

As far as the plenum volumes are concerned, one is placed between the compressor and the turbine, and the other between the turbine and the power turbine. The volumes are in a sense replacing the algebraic constraints, which were used earlier in the steady state model for guessing P_2 and π_t and satisfying both mass flow and work compatibility. These volumes are introduced for taking into account all the flow imbalances, given that in transient operating conditions only the flow compatibility is satisfied. The mass flow entering each individual component is assumed to be the same leaving it. The mass flow imbalances initiated by the fuel addition in the combustor are utilized for evaluating the rate by which pressure increases. A description of the engine dynamics follows in the next paragraphs.

2.3.1. Dynamics

Combustor: Volume 1. A simplified version of the law of continuity of mass is commonly used to describe the pressure rise within the combustor:

$$\frac{dP_2}{dt} = \frac{RT_2}{V_1}(\dot{m}_1 + \dot{m}_f - \dot{m}_3) \tag{15}$$

where R, V_1, and P_2 denote gas constant, combustor volume, and compressor delivery pressure, respectively. The combustor outlet pressure can be calculated as a simple proportionality from:

$$\frac{P_2 - P_3}{P_2} = PLF \tag{16}$$

where PLF is the combustor pressure loss factor and for this study a 5% drop in pressure is assumed.

Duct: Volume 2. For the duct volume between the turbine and the power turbine, the pressure of the gas generator turbine is given by:

$$\frac{dP_4}{dt} = \frac{RT_4}{V_2}(\dot{m}_3 - \dot{m}_4) \tag{17}$$

where V_2 and P_4 denote duct volume and turbine delivery pressure, respectively. The turbine outlet pressure can be calculated as a simple proportionality from:

$$\frac{P_4 - P_{45}}{P_{45}} = PLF \tag{18}$$

where PLF is the turbine pressure loss factor and for this study we assumed that there are no losses between the turbine and the power turbine, i.e. $P_4 = P_{45}$. In contrary to the combustor, in this volume there is no heat addition so that it can be assumed that temperature T_4 remains the same at the entry and the exit of this duct.

Shaft. Due to the fact that only flow compatibility is satisfied during transient conditions, the difference between the work consumed by the compressor W_c, and work extracted by the turbine W_t, is utilized to compute the acceleration/deceleration of the engine as follows:

$$\frac{dN}{dt} = \left(\frac{30}{\pi}\right)^2 \cdot \frac{W_t - W_c}{JN} \tag{19}$$

where J is the shaft polar moment of inertia measured in kg m^2.

System States. Let us assume that the set of variables which govern the dynamics of the system is denoted by x and the vector input that changes the system's state is denoted by u. For the dynamic engine model, the compressor and turbine exit pressures P_2 and P_4, can be considered as the states of the systems which are critical. If all the isentropic efficiencies and temperatures of the gas turbine components are determined, then the engine gas path pressures can be computed from thermodynamic equations. The shaft rotational speed N of the gas turbine is another critical state of the system. The fuel flow rate $\dot{m}_f$ is implemented for controlling the system's state. Thus, the state and control variables are defined as follows:

$$x = [P_2, P_4, N]^T \tag{20}$$

$$u = \dot{m}_f \tag{21}$$

The gas path pressures along with the shaft rotational speed of the steady state conditions serve as initial conditions of the dynamic engine model. To summarize, the gas turbine dynamics may be expressed as:

$$\frac{dx}{dt} = f(x, u) \tag{22}$$

2.3.2. Simulation Process

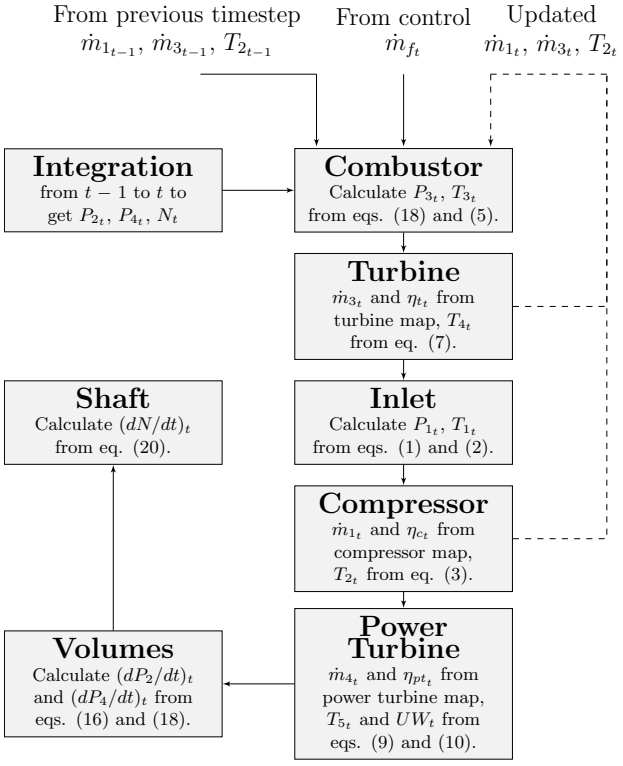

Figure 12: Flow chart of the engine model simulation process at transient conditions.

The flow chart of the simulation process is schematically represented in Fig. 12. As previously described, the ICV method has been employed for the transient performance analysis. A transient model has been also developed in Simulink environment. It shares the same architecture and component performance maps as the steady state model. The initial state values for the transient engine model are summarized in Table 2.

It should be stressed that during steady state operation all the derivatives dP_2/dt, dP_4/dt and dN/dt are equal to zero (i.e. $dP_2/dt = dP_4/dt = dN/dt = 0$). As long as the fuel flow supplied to the engine is not lying within the steady state operating line the work consumed by the compressor will not be matched by

Table 2: The initial state for the transient engine model.

Symbol	Parameter	Value	Units
P_{2_0}	compressor discharge pressure	1472	kPa
P_{4_0}	turbine exit pressure	406	kPa
N_0	gas generator shaft rotational speed	9000	rpm

the work extracted by the turbine. The engine will react to this unbalanced work by increasing/decreasing its shaft rotational speed, according to the fuel flow command.

2.4. Controller Design

Depending on the fuel flow command, the engine might be forced to operate in unfavorable conditions. Especially when there are sudden changes in the demanded shaft rotational speed, this could lead to violation of the engine firing temperature limits and even to compressor surge. This motivates the development of a suitable controller for ensuring that the fuel flow command will guarantee a safe and reliable engine operation.

Numerous control methods and controllers are available for gas turbine engines but for this study we implement a simple proportional plus integral (PI) controller to demonstrate its effectiveness. The PI controller is one of the most common controllers used in gas turbines and its objective is to regulate the fuel flow $\dot{m}_f$ according to the actuating signal ε arising from the comparison of the desired N_d and the measured N_m shaft rotational speed of the engine. One of the prerequisites for the design of a controller is to represent the behavior of the fuel flow actuator system and the speed measurement sensor. For the above purpose, the fuel flow actuator system and the speed sensor are both represented by first order transfer functions that are typical for these systems [25, 35].

The first transfer function acts on the input signal of fuel flow rate and the second one acts on the shaft rotational speed. The initial conditions of the transfer functions correspond to the mass flow rate and the shaft rotational speed at design point conditions. The controller receives the N_m signal and calculates the required fuel flow rate $\dot{m}_{f_d}$ by using the PI control schedule, and look-up tables for surge and flame out limits which are discussed in Case Study 2 of the Results Section. The demand of $\dot{m}_{f_d}$ is then turned into the actual fuel flow $\dot{m}_f$ injected into the engine combustor to maintain the engine operation. A simple schematic diagram of this arrangement can be seen from Fig. 13.

The control function of this PI controller can be expressed as follows:

$$\dot{m}_{f_d}(t) = K_p \varepsilon(t) + K_i \int_0^t \varepsilon(t) dt \tag{23}$$

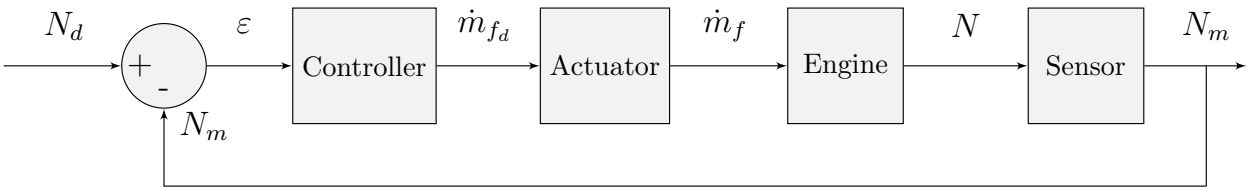

Figure 13: Block diagram of a speed controller for fuel flow regulation.

where $\varepsilon(t) = N_d(t) - N_m(t)$, and K_p, K_i denote the coefficients of the proportional and the integral terms, respectively. The transfer functions for the fuel system actuator and the speed sensor are given by:

$$G_1(s) = \frac{\dot{m}_f(s)}{\dot{m}_{fd}(s)} = \frac{1}{0.05s + 1} \tag{24}$$

$$G_2(s) = \frac{N_m(s)}{N(s)} = \frac{1}{0.05s + 1} \tag{25}$$

These simple first order lag equations are adequate for satisfying the objective of this analysis which is to demonstrate the effectiveness of a controller on the engine transient behavior. However, if a more detailed approach of engine controller design is sought then the reader is prompted to [35]. Based on the observations of the engine model behavior at transient conditions, we have developed a PI controller and tuned accordingly its coefficients K_p and K_i in order to obtain smooth operation of the engine model. The implementation of such a controller ensures smooth acceleration and deceleration of the engine.

2.5. Validation

PROOSIS [43] gas turbine simulation software has been used for validation. PROOSIS is based on the EL (Ecosim pro Language) and has been tested for numerous power and propulsion applications [49].

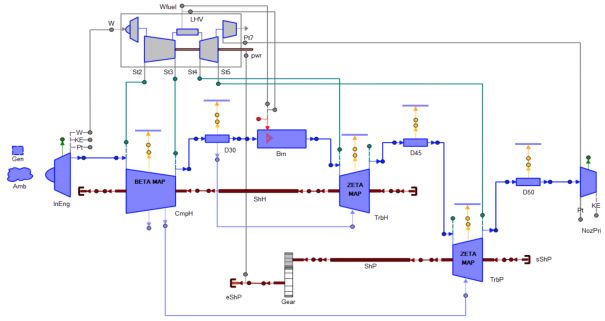

Figure 14: Engine model layout in the PROOSIS environment.

A similar gas turbine engine system has been modeled in PROOSIS environment for validating the developed Simulink engine model. A schematic layout of the assembled engine model in PROOSIS environment is shown in Fig. 14.

2.6. Wind Turbine Model

For assessing the dynamic performance behavior of the gas turbine model in a hybrid gas/wind power plant, a set of wind turbines have been simulated in MATLAB/Simulink.

For this study, a generic wind turbine model available from MATLAB/Simulink environment [50], which is based on [51], has been used to demonstrate the effect of variable wind speed in the power extracted from a set of wind turbines. Consequently, the gas turbine has to operate under transient conditions to satisfy the fluctuating power demanded from this hybrid power plant.

The main parameters that govern the performance of a wind turbine are pitch angle β, wind speed V_{wind} and wind turbine generator speed N_{wt}. The interrelationships of the above parameters are schematically represented in a wind turbine performance map, as seen in Fig. 15. The power output of a wind turbine UW_{wt} is expressed as follows [51]:

$$UW_{wt} = \frac{1}{2} \cdot \rho \cdot A \cdot C_p \cdot V_{wind}^3 \tag{26}$$

where ρ denotes the air density, A denotes the turbine swept area, and C_p denotes the power coefficient. The power coefficient C_p is a function of blade tip ratio λ and the blade pitch angle β. For this study a generic equation is used as follows [51]:

$$C_p(\lambda, \beta) = C_1(C_2/\lambda_i - C_3\beta - C_4)e^{\frac{-C_5}{\lambda_i}} + C_6\lambda \tag{27}$$

where $C_1 = 0.5176$, $C_2 = 116$, $C_3 = 0.4$, $C_4 = 5$, $C_5 = 21$, and $C_6 = 0.0068$. The blade tip ratio relationship with pitch angle is given by:

$$\frac{1}{\lambda_i} = \frac{1}{\lambda + 0.08\beta} - \frac{0.035}{\beta^3 + 1} \tag{28}$$

The wind turbine model has three inputs namely β, V_{wind}, N_{wt}, and one output UW_{wt}.

The hybrid gas/wind power plant consists of a gas turbine and a wind farm with variable power output. The total power output UW_{total} from the hybrid power plant is given by:

$$UW_{total} = UW_{gt} + UW_{wt} \tag{29}$$

The objective of the gas turbine is to fill the gap between the demanded power DW and the power output of the wind turbine UW_{wt}. The difference ΔW between total power output UW_{total} and demanded power DW is as follows:

$$\Delta W = DW - UW_{total} \tag{30}$$

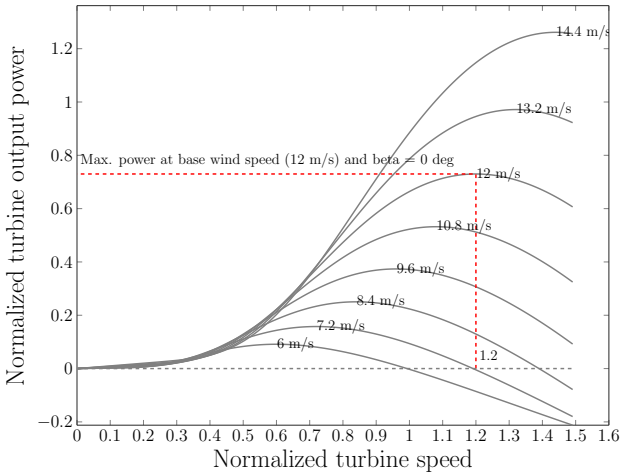

Figure 15: Wind turbine performance map representing the power output as a function of generator speed, for different wind speeds and for a blade pitch angle β= 0 degrees.

Now if $\Delta W \neq 0$ then demand is not satisfied, and another operating point should be chosen for the gas turbine, in order to ensure that the power output of the hybrid power plant meets the power demand, i.e. $\Delta W = 0$. To simulate this effect, we implement an algebraic constraint which aims to minimize ΔW by changing the demanded shaft rotational speed from the gas turbine N_d. The speed demand N_d signal is then transmitted to the controller which regulates the fuel flow $\dot{m}_{f_d}$ of the gas turbine for minimizing ΔW.

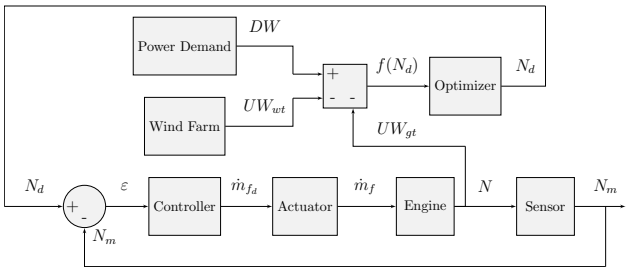

Figure 16: Block diagram of the hybrid gas/wind controller and optimization module.

This algebraic constraint optimizes the selection of N_d, which in turn affects the feedback computation of ΔW which acts as the input to this block, i.e. $f(N_d) = \Delta W$. It should be pointed out that the wind turbine implemented here is a simple model tailored for this study, which focuses more on the performance assessment of the gas turbine in a hybrid gas/wind power plant. However, if one pursues a high fidelity analysis of a wind turbine for its integration into a hybrid wind/gas turbine plant then the reader is prompted to studies [52, 53, 54, 55], which explore in a more detailed fashion the dynamic behavior and control of wind turbines.

3. Results and Discussion

3.1. Case Study 1: Steady State

The objective of this Case Study is to examine the behavior of the engine at design point and off-design steady state conditions. So starting from its design point performance, which is summarized in Table 3, the engine is modeled for various shaft rotational speeds for a 10 seconds simulation run time. The engine model is a generic two-shaft gas turbine as it does not refer to a specific engine. Its power capacity places it between Siemens SGT-600 and GE LM2500+. In case that a particular engine is sought to be modeled, linearly scaled versions of available compressor and turbine maps will suffice for design point simulations. On the other hand, for off-design performance studies, non-linear tuning of the maps could be performed [56] for matching the model to the targeted gas turbine engine.

The time step of the simulation is set to 1 second. The steady state modeling is a discrete simulation so a different shaft rotational speed corresponds to each time step. The nominal value of N at time instant t=0 seconds is 9,000 rpm and is reduced 300 rpm/s, such that at the time instant t=10 seconds, the shaft rotational speed is 6,000 rpm. This results in 11 operating points covering a wide range of gas generator shaft speeds.

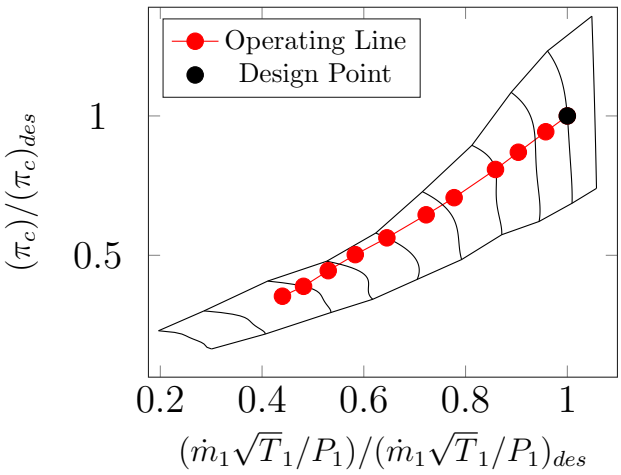

Figure 17: The compressor map operating line at steady state conditions.

The collection of the steady state operating points is fundamental in determining the operating line of the engine and present it in the compressor map chart. It is clear from Fig. 17, that the engine operating points are not exceeding the surge line of the compressor. However, at the lower than nominal speed regions, the operating line approaches the surge line. If the initially assumed zero inlet pressure losses are accounted for, then surge might be a possibility. Generally, the surge margin should be approximately 20% [41] for establishing a reasonable threshold, beyond which the engine would not be allowed, by the control system,

Table 3: The design-point performance specifications of the engine model.

Symbol	Parameter	Value	Units
P_a	ambient pressure	101	kPa
P_1	compressor inlet pressure	101	kPa
P_2	compressor discharge pressure	1,472	kPa
P_4	turbine discharge pressure	406	kPa
P_5	power turbine discharge pressure	101	kPa
T_a	ambient temperature	288	K
T_1	compressor inlet temperature	288	K
T_2	compressor discharge temperature	670	K
T_3	turbine entry temperature	1,372	K
T_4	turbine exit temperature	1,044	K
T_5	power turbine exit temperature	779	K
η_i	inlet efficiency	1	-
η_c	compressor efficiency	0.86	-
η_m	mechanical efficiency	1	-
η_t	turbine efficiency	0.87	-
η_{pt}	power turbine efficiency	0.86	-
$\dot{m}_1$	inlet mass flow rate	87.70	kg/s
$\dot{m}_f$	fuel flow rate	1.68	kg/s
$\dot{m}_4$	exhaust flow rate	89.38	kg/s
UW	power output	27.1	MW
N	gas generator shaft rotational speed	9,000	rpm
N_{pt}	power turbine shaft rotational speed	6,000	rpm
LHV	low heating value of fuel	42,000	kJ/kg

to operate. The compressor surge limit has been taken into account and integrated into the controller subsystem. A detailed description of the above is provided in Case Study 2 of the Results Section.

The variation of the monitored engine parameters with respect to the shaft rotational speed can be seen from Fig. 18. It is evident that the selected measurements follow the same trend as rotational shaft speed changes. It is worth noting that the steady state engine model is crucial for the initialization of the dynamic engine model which is described in the next section.

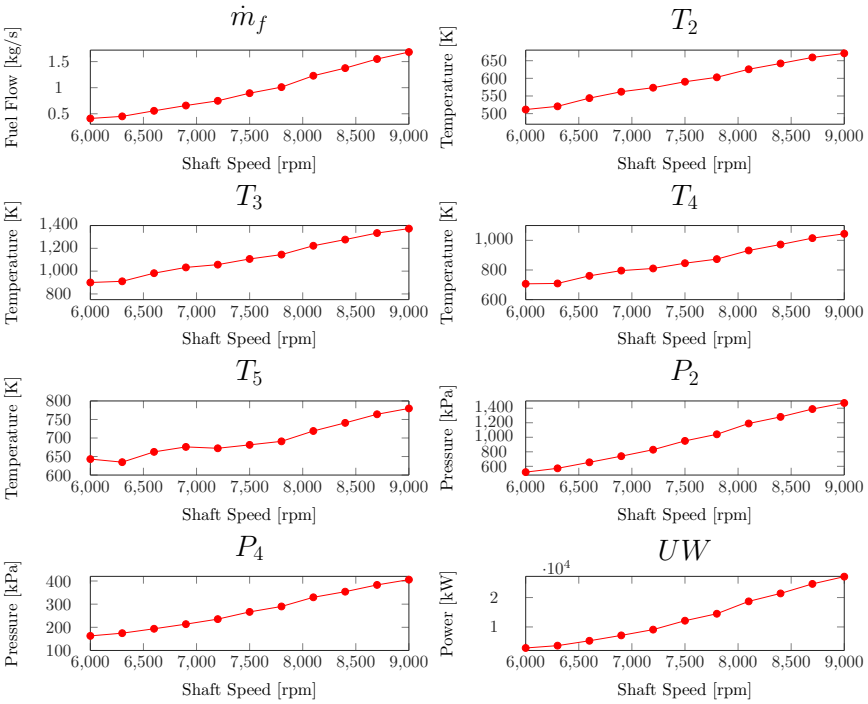

Figure 18: Simulated measurements of the engine model at steady state conditions.

3.2. Case Study 2: Transient Step Response

The objective of Case Study 2 is to analyze the engine model performance for step fuel flow commands. Before finalizing the transient engine model, a sensitivity analysis has been carried out to evaluate the impact that both volumes V_1, V_2 inserted between the components, and the shaft inertia J, have in the model. As it can be seen from Fig. 19, for a step fuel flow command the transient engine model is more sensitive to variation of shaft inertia than that of the inter-component volume size.

The shaft inertia is related to the size of the gas turbine and varies from engine to engine. A heavy duty gas turbine has a higher shaft inertia than a micro gas turbine. This means that a heavy duty engine will have a slower response to transient maneuvers in comparison to a micro gas turbine. The above is observed from the examined sensitivity analysis, where the response time of the transient model decreases as the shaft inertia increases. To overcome this limitation, heavy duty gas turbines might incorporate variable geometry compressors that allow them to operate more flexible and meet fluctuating demand. For this gas turbine model the values selected for the inter-component volumes and the shaft inertia are summarized in Table 4. These values represent a fast and highly dynamic engine model, which presents greater challenges in terms of controller design than a slower engine model which is characterized by a higher shaft inertia value. In addition, the above assumption aids the simulation of plethora of scenarios in a shorter time frame. Nevertheless, if the information of a gas turbine's shaft inertia is known then the model can be easily

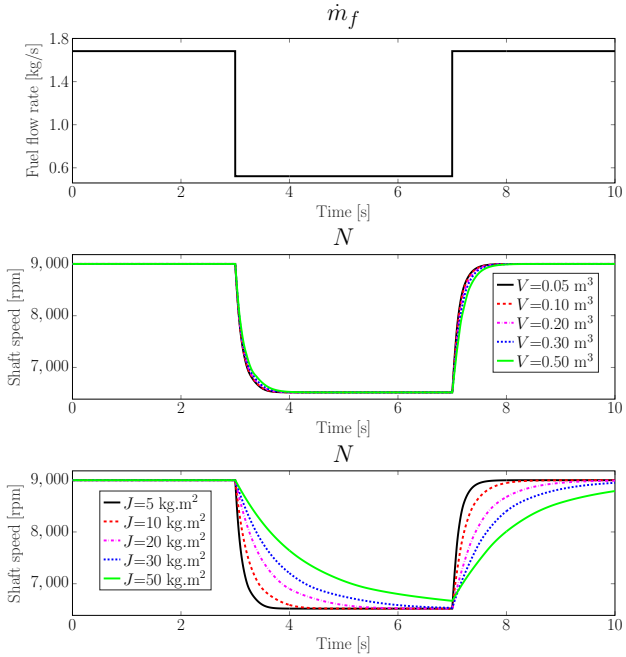

Figure 19: Sensitivity analysis of transient engine model to inter-component volumes and shaft inertia.

updated with these specifications.

Table 4: Selected values for inter-component volumes and shaft inertia.

Parameter	Value	Units
V_1	0.05	kg/m^3
V_2	0.05	kg/m^3
J	5.0	kg m^2

The engine model arrangement for this Case Study represents an open-loop control system since there is no controller implementation. For this Case Study the fuel flow, shown in Fig. 21, commences at time instant t=0 seconds from its steady state condition until it reaches time instant t=3 seconds.

At t=3 seconds, a step input is utilized to instantly decrease fuel flow to 70% of its design point value. The fuel flow command will be maintained at this level for another 4 seconds until t=7 seconds, where it will step back to its original steady state condition for the remaining simulation.

For the step fuel flow command the acceleration/deceleration trajectories on the compressor map are seen in Fig. 20. The step command accesses a large area in the compressor map and such fast commands might force the engine to operate closer to surge and stall.

The assessment of the engine performance during fast step responses provides useful insights about the

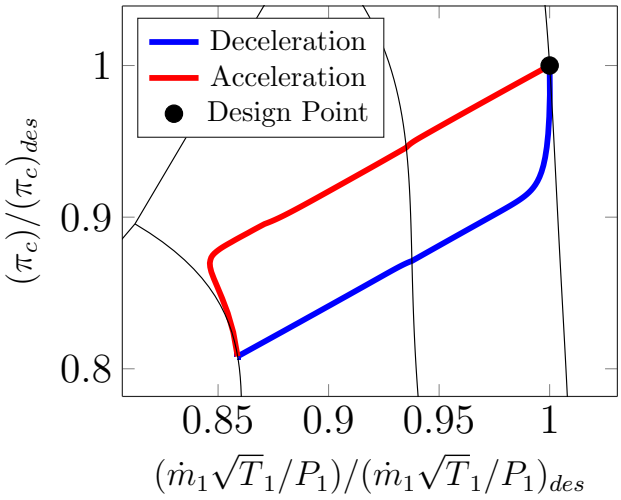

Figure 20: Representation of the compressor map trajectories during the transient step response of the dynamic engine model.

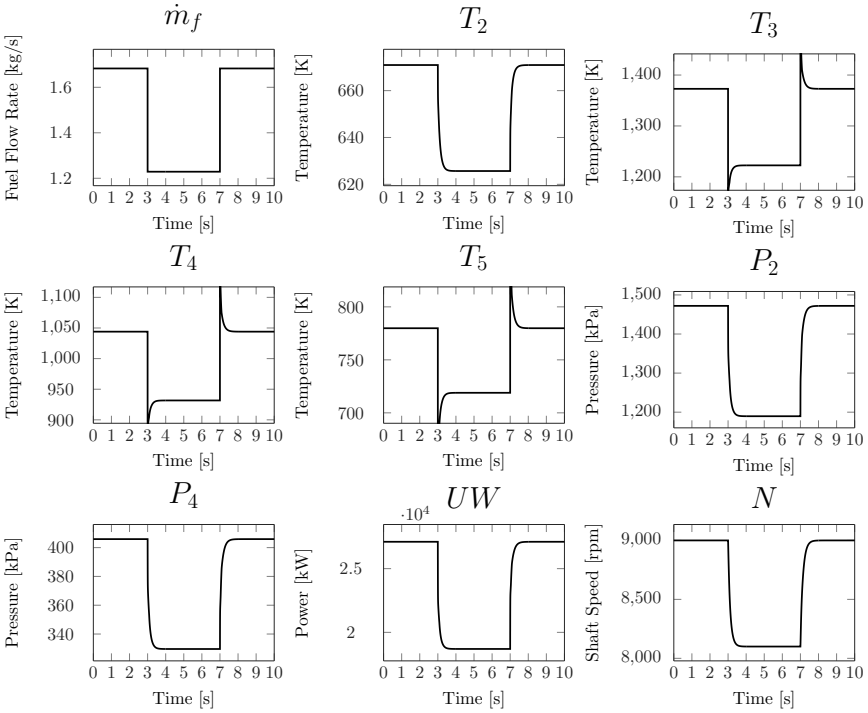

Figure 21: The simulated parameters of the dynamic engine model with respect to time for a step fuel flow command.

operating and surge limits of the engine that could subsequently facilitate the development of a controller. A close examination of the measured parameters, seen in Fig. 21, demonstrates that the response of the engine to this step command results in sudden temperature changes to the hot end of the engine. These are reflected by the temperatures at turbine entry T_3, turbine exit T_4, and power turbine exit T_5. In practice, unregulated fuel flow commands such as these might prove catastrophic for the engine since they might

violate its firing temperature limits and lead to compressor surge. These types of observations and insights promote the importance of transient performance analysis of an engine.

Towards this end, a simple approach has been carried out in order to assess the engine's limitations to fast transient maneuvers. During fast acceleration and deceleration, the engine may experience compressor surge and combustor flame-out, respectively. To simulate these phenomena, the fuel flow command is decreased in a step manner and approaches minimum fuel flow rate before stepping up again and stabilizing in steady state conditions. By examining the trajectories of this maneuver, from the compressor map, seen in Fig. 22a, it becomes clear that during deceleration the operating line is displaced to the lower boundaries of the compressor map while in the acceleration phase the operating points lie in close proximity to the surge line.

For fuel control purposes, it is a common practice to express the corrected fuel flow rate $\dot{m}_f/\left[(P_1/P_{1_{ref}})(\sqrt{T_1/T_{1_{ref}}})\right]$ with respect to the corrected rotational speed $N/(\sqrt{T_1/T_{1_{ref}}})$. This results in a fuel flow envelope, which represents the variation of engine steady running line, flame-out limit and surge limit, as seen from Fig. 22b.

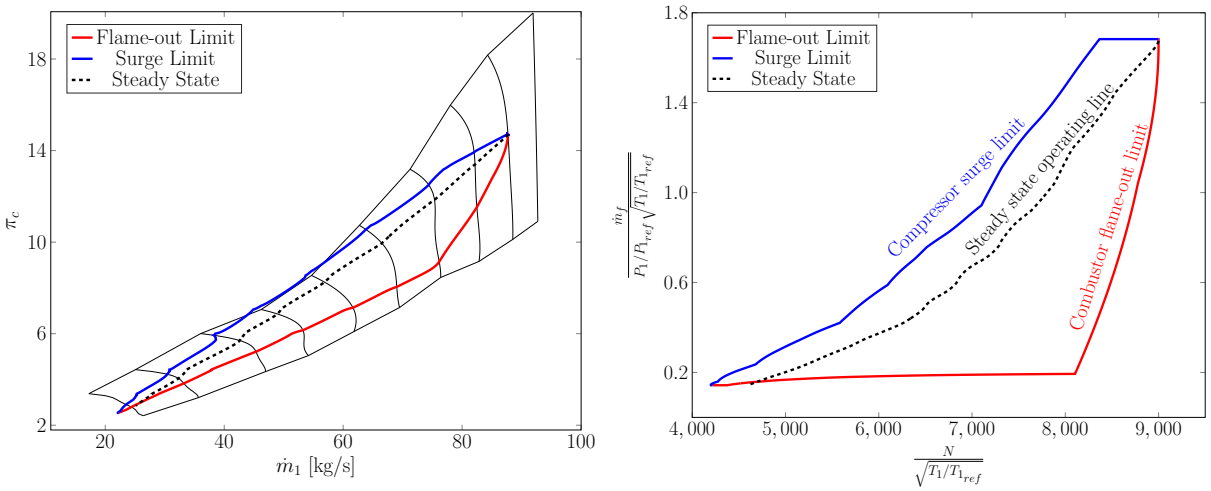

(a) Compressor map trajectories for steady state, acceleration and deceleration.

(b) Fuel flow rate variation with respect to shaft speed for steady state, acceleration and deceleration.

Figure 22: Representation of surge and flame-out limiting functions during steady state, acceleration and deceleration of the engine model.

From Fig. 22b, it can be seen that in order to change engine power settings the fuel flow must be controlled in such a manner so to avoid crossing the surge and flame-out boundaries.

It can be concluded that fast and accurate preliminary model-based evaluation of the transient engine behavior has the prospect of saving costs by avoiding tests that might lead to engine failure and more importantly to facilitate the design of controllers for establishing the safe operating limits of a complex and highly nonlinear system.

3.3. *Case Study 3: Transient Step Response with* PI *Controller*

The objective of this Case Study is to assess the effect of a simple PI controller under transient conditions. Specifically, a PI controller is used to regulate the fuel flow and ensure a smooth acceleration and deceleration of the engine. The schematic diagram of this control arrangement is shown in Fig. 23.

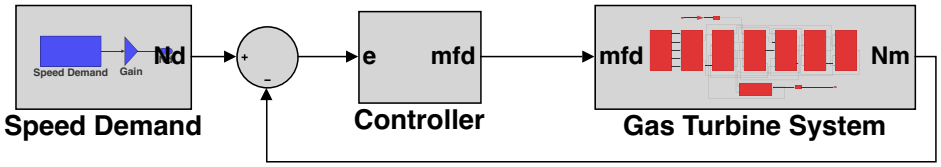

Figure 23: Schematic layout of the MATLAB/Simulink model with the controller.

The PI controller modifies the fuel flow based on the difference between measured N_m and demanded N_d shaft speed of the engine. The coefficients K_p and K_i of the controller have been tuned from the built-in tuning function of Simulink. In this environment, the user has the capability to observe the initial response of the engine block. Moreover, the visual representation of the system's tuned response enables the user to properly identify the desired transient response characteristics of the engine. This process results in a set of tuned coefficients that subsequently update the PI controller used in Simulink model.

The operating limits of the engine model, established in Case Study 2, are also integrated into the controller subsystem, as seen in Fig. 24.

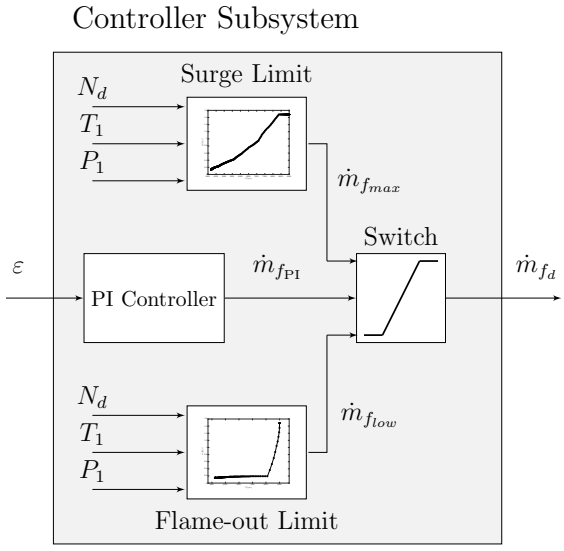

Figure 24: Detailed block diagram of the controller subsystem with the surge and flame-out limiting functions implemented as look-up tables.

The controller has to regulate the fuel flow into the engine by ensuring that this command lies within the surge and flame-out limits. So depending on the demanded shaft speed N_d and the ambient conditions

T_1, P_1, two look up tables are utilized to determine the maximum $\dot{m}_{f_{max}}$ and minimum $\dot{m}_{f_{low}}$ fuel flow rate limits that correspond to surge and flame-out, respectively. If the fuel flow rate $\dot{m}_{f_{\mathrm{PI}}}$ computed by the PI controller crosses the above two limits, then a switch is used that ensures that the final fuel flow demand $\dot{m}_{f_d}$ will always lie within these limits. In any case where the controller has other limiting functions these can be easily integrated in the same control layout.

For this Case Study, the coefficients of the PI controller and the transient response characteristics are summarized in Table 5.

Table 5: The parameters of the PI controller.

Parameter	Value	Units
K_p	8.562E-05	-
K_i	0.794E-03	-
Rise time	0.896	seconds
Settling time	1.676	seconds
Overshoot	0	%
Peak	1	-

Repeating the simulation of the engine model in Simulink results in a controlled engine behavior. A comparison between the behavior of the engine model of Case Study 2 Case Study 3 which implements the PI controller is seen in Fig. 25.

It becomes clear from Fig. 25, that T_3 is no longer exhibiting an oscillating behavior during this sudden increase in the demanded engine speed, since the fuel flow has been modified through the PI controller. At this point it is important to demonstrate the effectiveness of the PI controller by comparing the fuel flow rate $\dot{m}_f$ with respect to the shaft rotational speed N for the controlled and uncontrolled engine model as seen from Fig. 26.

It is evident from Fig. 26, that for Case Study 2 where the fuel flow command was not regulated by a controller, a large operational regime is occurred that would have violated the firing temperature limits and may have led to compressor surge. The implemented controller has resolved the previous issues of Case Study 2 by regulating a fuel flow rate that results in a smoother engine operating profile.

3.4. Case Study 4: Validation with PROOSIS for Fuel Schedule 1

Two different fuel flow schedules are implemented to establish a variety of dynamic operating conditions for which Simulink engine model can be validated. The comparison is facilitated by the fact that the fuel flow schedules for PROOSIS and Simulink models are identical. A 5 seconds simulation run time with a time step of 1 milliseconds is selected for Case Studies 4 and 5.

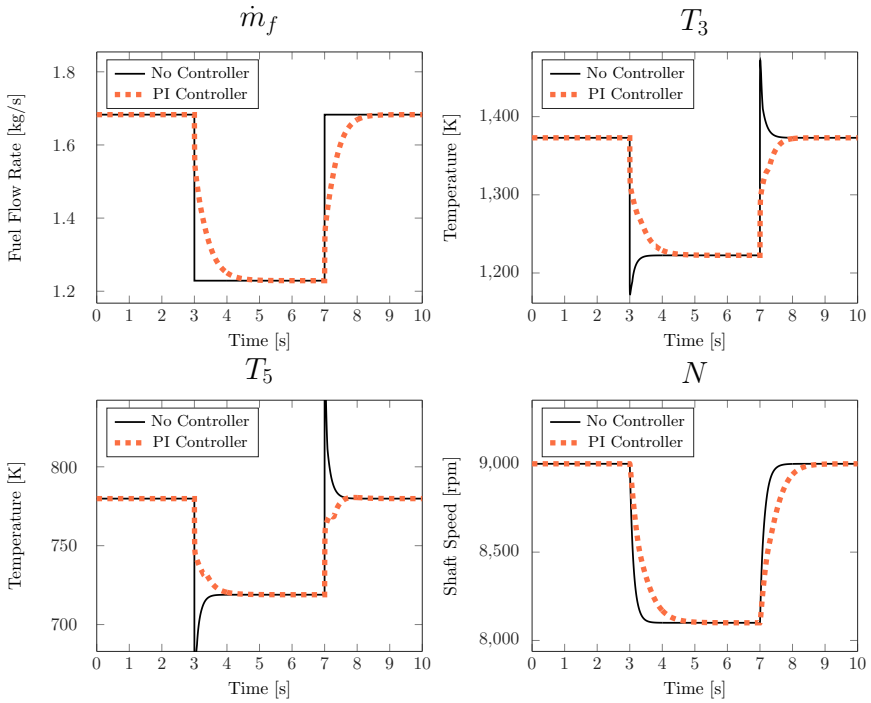

Figure 25: Variation of the simulated measurements with respect to time from MATLAB/Simulink model of Case Study 3.

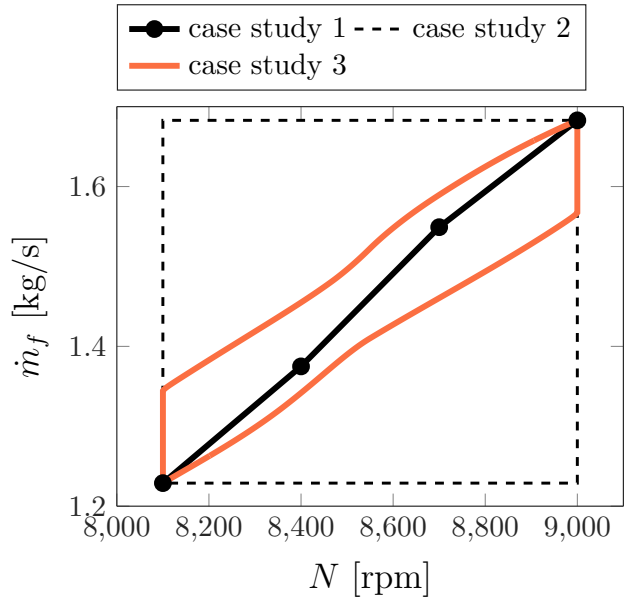

Figure 26: The variation of the fuel flow rate $\dot{m}_f$ with respect to the shaft rotational speed N for Case Studies 1,2 and 3.

Since the objectives of both Case Studies 4 and 5 is to validate the developed engine model's accuracy, a group of performance parameters are selected. Engine parameters such as power output UW, power turbine exit temperature T_5, compressor discharge temperature T_2, pressure P_2, shaft rotational speed N, and their

variations with respect to time are examined. The simulation results and the prediction error for Case Study 4 are shown in Figs. 27 and 28, respectively.

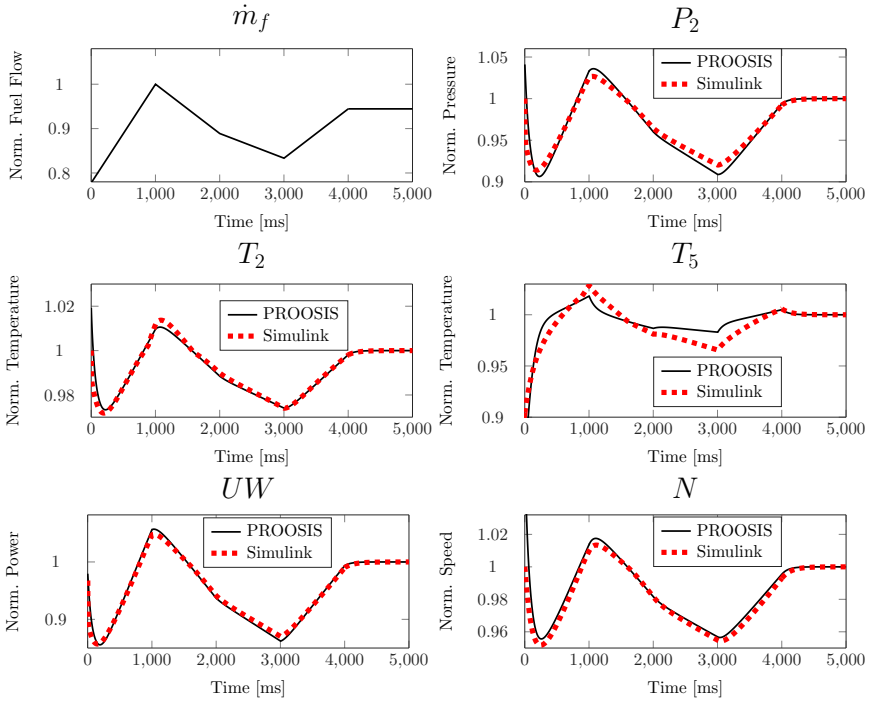

Figure 27: Variation of the simulated measurements with respect to time from Simulink and PROOSIS models of Case Study 4.

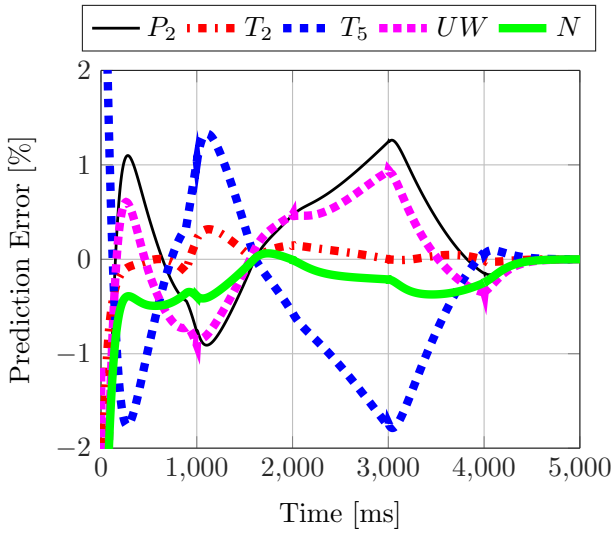

Figure 28: Prediction error of Simulink model measurements with respect to the PROOSIS model for Case Study 4.

The selected parameters are presented in normalized (to design conditions) form to facilitate the compar-

ison. The first observation from this Case Study is that the Simulink model is having a good agreement with PROOSIS as reflected by the comparison of their performance parameters. The parameters that are most accurately matched with PROOSIS are compressor discharge temperature T_2 along with power output UW and shaft rotational speed N. The compressor discharge pressure P_2 and the power turbine exit temperature T_5 present a maximum error of approximately 1.5% in certain regions.

3.5. Case Study 5: Validation with PROOSIS for Fuel Schedule 2

In this Case Study, we simulate a different fuel command than the one of Case Study 4, as seen from Fig. 29. The primary aim of this study is to verify the repeatability of the earlier validation. The fuel flow command has an initial setting corresponding to steady state conditions, and at t=2 seconds there is a small drop to 87% of its nominal value which is then followed by a fuel flow increase for 1 second before it stabilizes again for the remaining simulation at 94%. The simulation results and the prediction error for Case Study 5 are shown in Figs. 29 and 30, respectively.

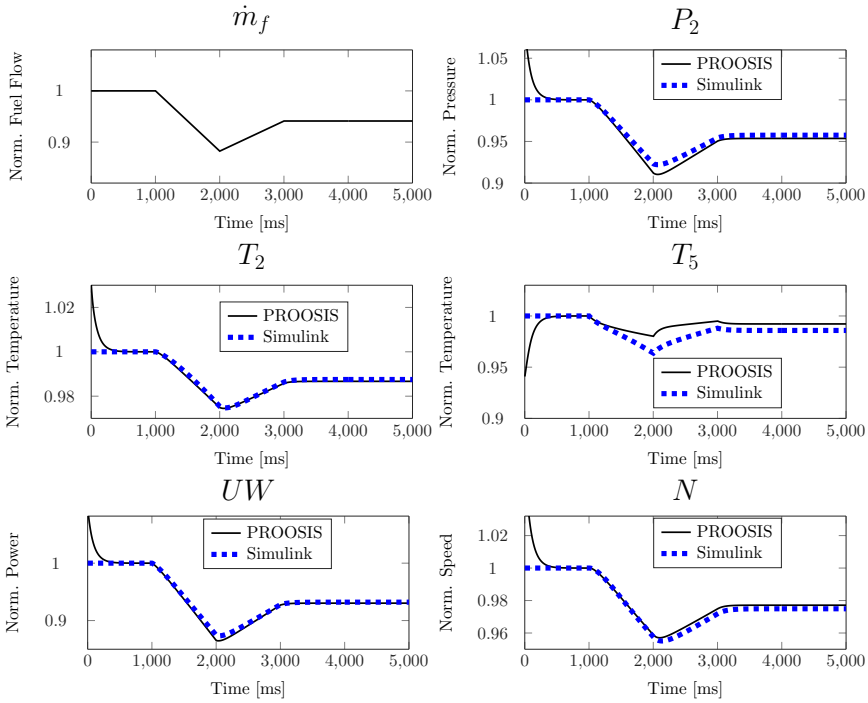

Figure 29: Variation of the simulated measurements with respect to time from Simulink and PROOSIS models of Case Study 5.

It is noted from Fig. 29, that it takes almost 200 iterations for the model in PROOSIS to overcome the initial transient effects, which occur due to mass flow accumulation inside the volumes, before reaching a steady state condition. On the other hand, Simulink model does not exhibit such an effect since its initialization process was facilitated by the steady state model developed. It follows that the Simulink model

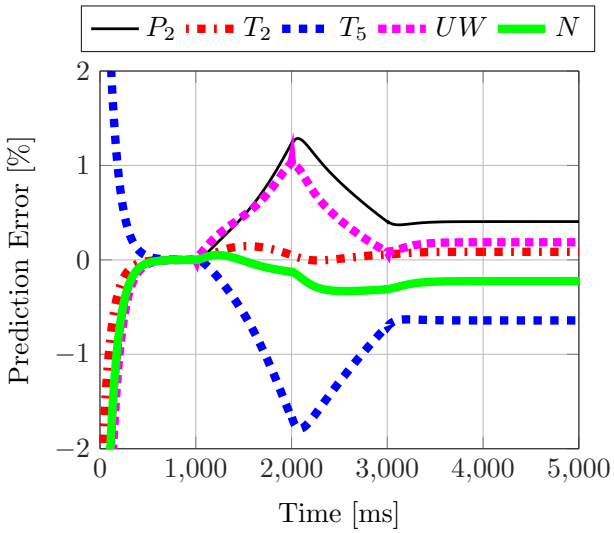

Figure 30: Prediction error of Simulink model measurements with respect to the PROOSIS model for Case Study 5.

is of similar accuracy to PROOSIS. All the simulated parameters of Simulink model in Case Study 5 follow the same trends with PROOSIS model, and the maximum prediction error in P_2 and T_5 is approximately 1.7%.

This error discrepancy observed in both P_2 and T_5 is probably due to the different method that each program uses in the initialization procedure. It seems that it takes significantly more time for PROOSIS to stabilize in the design point conditions compared to Simulink. This means that the initial guesses used in the component matching process might be slightly off from the design point conditions. Consequently, the chosen operating points in the performance maps lead to the under-prediction of P_2 and over-prediction of T_5, which both compensate to satisfy the selected design point.

The Simulink model converges instantly and without any hysteresis in a new power setting. Since the developed engine model follows the same trend as that of PROOSIS data at a high level of accuracy it substantiates the method's validity.

The mean prediction error for both Case Studies 4 and 5 is seen in Fig. 31. The Simulink engine model has a mean error in T_5 which is equivalent to 6 K for a nominal value of 779 K. This emphasizes the model's accuracy which can form the basis for controller design and model-based fault diagnostics and prognostics. As far as the the mean error in the power output, this is approximately 0.4% which is equivalent to 108 KW for a nominal power output of 27.1 MW.

Finally, for the shaft rotational speed the mean error is 0.2% which is equivalent to 18 rpm for a nominal N of 9,000 rpm. Another important aspect worth of consideration is the computation time. For a 5 seconds run, the Simulink model converges in 0.24 seconds, when the simulation is performed in a PC with an Intel Core i5 of 2.4 GHz and 4GB of RAM.

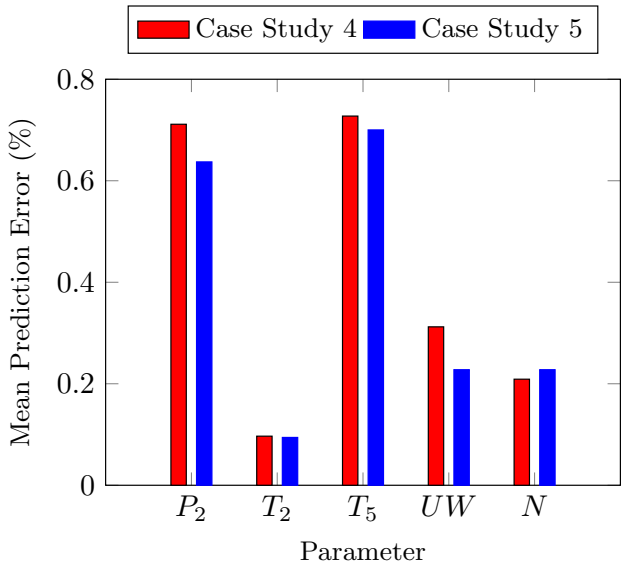

Figure 31: Mean prediction error of Simulink model measurements with respect to the PROOSIS model for Case Studies 4 and 5.

Table 6: Computational time for Simulink and PROOSIS models.

Parameter	Simulink	PROOSIS	Unit
Simulation time	5.0	5.0	seconds
Time step	1	1	milliseconds
Run time	0.24	52.05	seconds
Run time/Time step	0.048	10.41	milliseconds

The run time for the PROOSIS simulation is 52.05 seconds using the same machine. The main reason for this increased computational time lies in the iterative procedure employed at the beginning of the simulation for the component matching. This difference is further amplified by comparing the run time per time step, as shown in Table 6, where Simulink model is significantly faster than PROOSIS.

The validation process carried out here can be further improved by implementing inverse modeling adaptation methods [15, 57, 56] in order to minimize any deviations between Simulink and PROOSIS.

The developed engine model has the capability of representing accurately the dynamic gas turbine behavior. The program is flexible and modular enough to facilitate the integration of controllers, model adaptation methods, variable compressor scheduling along with diagnosis and prognosis tools. Therefore, the user is capable of having a detailed assessment of the engine's dynamic response.

3.6. Case Study 6: Hybrid Gas/Wind Power Plant

In this Case Study we examine the dynamic behavior of the gas turbine when integrated into a hybrid plant consisting of wind turbines. A built-in MATLAB/Simulink model of a wind turbine has been used for this purpose. The nominal performance specifications of the wind turbine are summarized in Table 7 and these refer to a generic model available in [51].

Table 7: The design-point performance specifications of the wind turbine.

Symbol	Parameter	Value	Units
V_{wind}	wind speed	12	m/s
N_{wt}	generator speed	1800	rpm
UW_{wt}	power output	1500	kW

Let us now describe how the data are produced for this Case Study. The Simulink iteration step selected is 1 millisecond. The total run time is 10 seconds and the model generates 10,000 data points. Given that the focus of this study is to assess the behavior of the hybrid power plant for a 10 hour period, the available results should be correlated to represent this time interval. It is therefore assumed that 16 operating points correspond to one minute of operation. The vast amount of generated data samples ensure that the nonlinear behavior of the gas turbine engine is well captured during this analysis.

The hybrid gas/wind power plant model, seen in Fig. 32, consists of a gas turbine and a wind farm of 14 wind turbines. The simulated wind speed varies with respect to time and it ranges from 6 m/s to 15 m/s, as seen in Fig. 33a. The chosen profile of wind speed is intentionally designed in such a way so that in the beginning of simulation the gas turbine operates close to its design point, where model initialization has been performed. Once the wind speed starts to ramp up, at 2 and 5 hour marks, the engine will be forced to decelerate as fast as possible and follow on the wind turbines.

The primary aim of this study is to assess the dynamic response of the gas turbine while collaborating with the wind farm to satisfy the demanded power. For this purpose the gas turbine has to operate under transient conditions since the wind speed and the power demand vary with respect to time simultaneously, as shown in Figs. 33a and 33b, respectively. The power demanded from the hybrid power plant ranges from 28 MW up to 37 MW. At the same time the variation of wind speed, alters the performance of the wind farm in terms of its capacity, and the combined effect of the above two key variable parameters is illustrated in Fig. 33b.

The controller discussed in Case Study 3 is utilized here in combination with the algebraic constraint optimizer. The role of the algebraic constraint is to translate the difference between power output and demanded power, into a signal of shaft rotational speed which governs the PI controller architecture. The

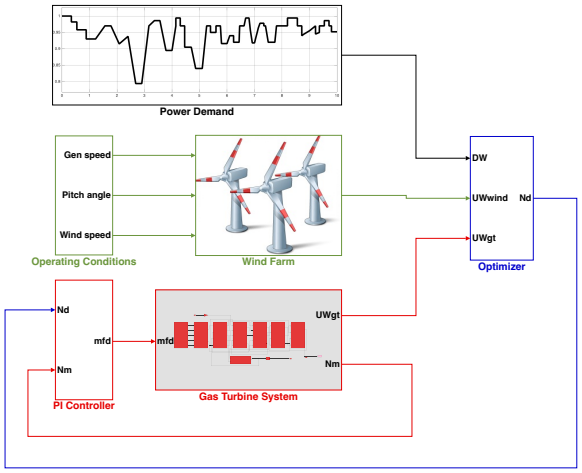

Figure 32: Schematic layout of the hybrid gas/wind power plant in Simulink.

properties of the PI controller are the same as in Case Study 3 while the simulation time for this Case Study is 10 seconds.

Figure 33c shows the remarkable variation in the power output from the wind turbines and the gas turbine as a percentage of the power demand. It is noted from Fig. 33c, that the wind farm has the capacity to contribute up to 70 % of the power demanded from the hybrid power plant while the maximum contribution from the gas turbine reaches 75%. Under these dynamic conditions, the performance behavior of the gas turbine is represented by the variation of shaft rotational speed N and exhaust gas temperature T_5, as seen in Figs. 34 and 35, respectively.

It is evident from Fig. 34 that the fluctuation of gas turbine's shaft rotational speed depends on wind speed which in turn governs the performance of wind turbines. A similar pattern is exhibited by the exhaust gas temperature of the gas turbine, as noted from Fig. 35, where the gas turbine operates under fast transient conditions to fill the energy gap imposed by the wind turbines power output.

3.7. Case Study 7: Hybrid Power Plant Comparison with a Twin Gas Turbine Plant

The objective of this Case Study is to compare the performance of the hybrid gas/wind power plant with a plant that consists of two gas turbines. For facilitating their comparison, the hybrid gas/wind power plant is referred as Plant A and the twin gas turbine plant as Plant B. The gas turbines of Plant B are identical to the gas turbine of Plant A. The power demanded from each plant is identical and within a time frame that corresponds to 10 hours of operation the performance of each plant is evaluated and NO_x emissions and fuel consumption are also assessed. The power demanded from each plant can be seen in Fig. 36.

It should be noted that the demanded power signal has been designed in such a way so that there are two occasions during which the power drops significantly and peaks up again. This is done intentionally, as

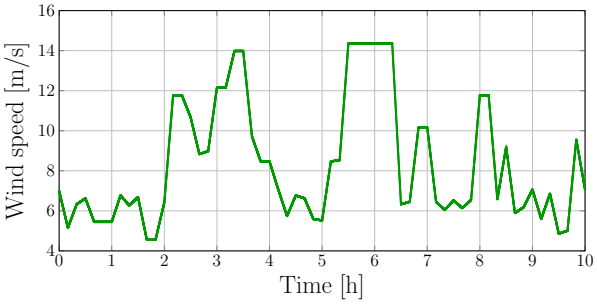

(a) Variation of wind speed with respect to time.

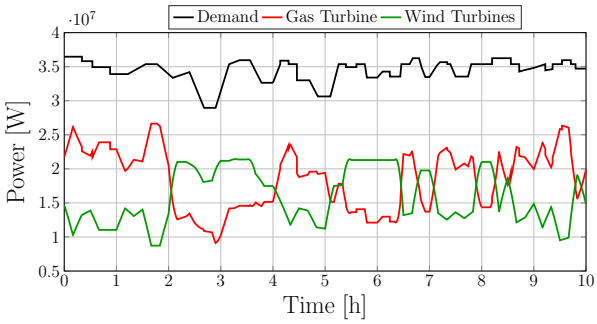

(b) Time response of the gas turbine and the wind turbines to meet the fluctuating demand.

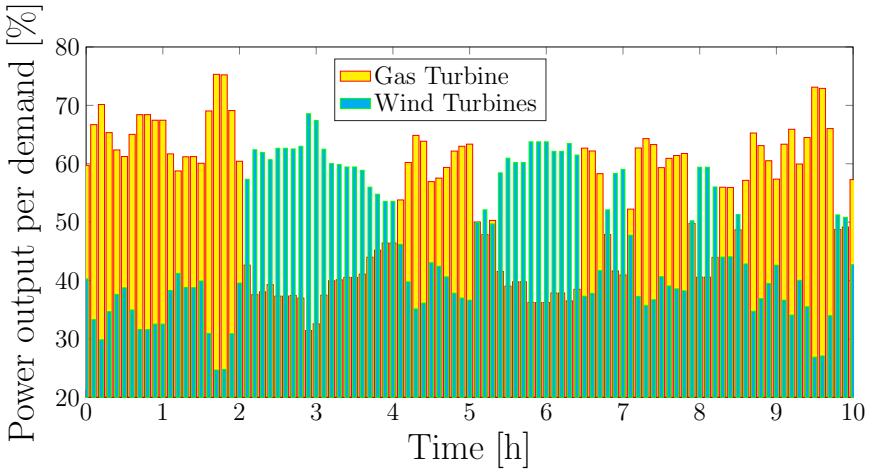

(c) The variation of the power output from the gas and wind turbines expressed as a percentage to total power demand with respect to time.

Figure 33: Time responses of the hybrid power plant components with respect to time.

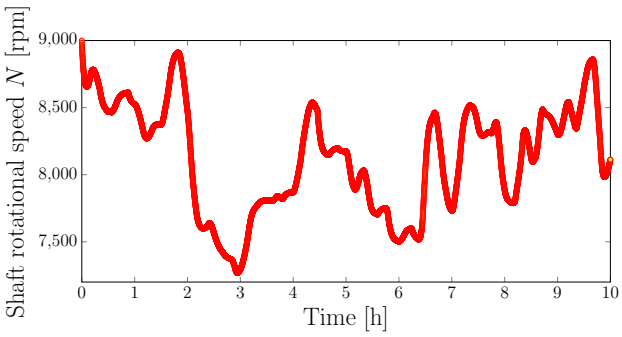

Figure 34: The variation of the gas turbine shaft rotational speed with respect to time.

we want to evaluate the shut down capability of the gas turbine used in Plant A. Generally, the capacity of the wind turbines is insufficient to satisfy the demanded power so the gas turbine has to support the wind

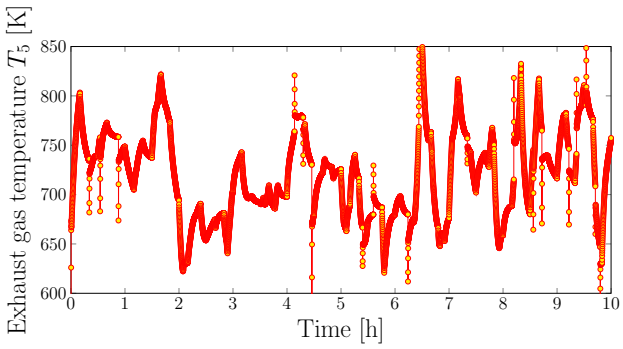

Figure 35: The variation of the gas turbine exhaust temperature with respect to time.

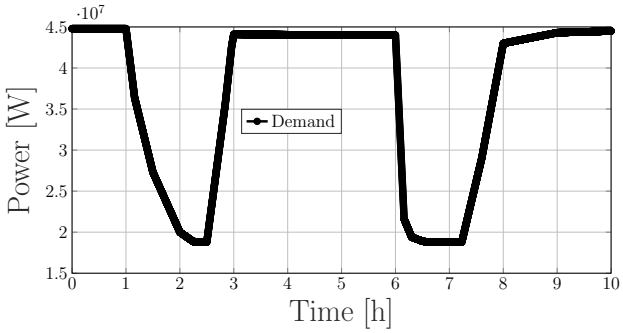

Figure 36: Representation of power demanded from Plants A and B with respect to time.

farm by fulfilling the energy demand as fast as possible.

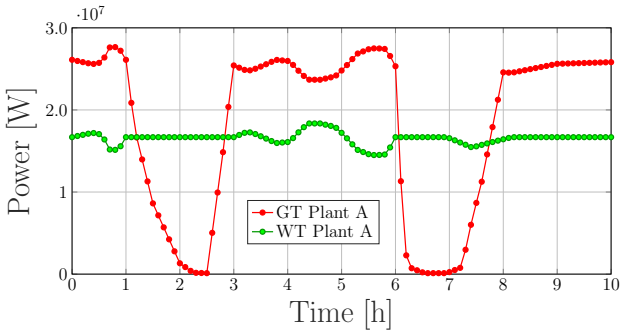

Figure 37: The variation of the power output from the gas and wind turbines of Plant A expressed with respect to time.

As it can be seen from Fig. 37, the gas turbine of Plant A operates close to its design point. After 1 hour of operation, the power required from the engine decreases slowly with respect to time and forces the engine to shut down and remain inactive for 30 minutes. It then starts up again and in approximately 25 minutes reaches a power setting close to its design point for the next 3 hours. At the 6 hour mark, the power output reduces faster as it takes approximately 10 minutes to shut down the engine.

Generally, modern gas turbine engines are capable of shutting down in less than 10 minutes [58]. On

the other hand, a hot start up (i.e. less than 8 h standstill) process may take less than 0.1 hours (i.e. 6 minutes) with a ramp rate up to 15% of nominal load per minute [59]. The acceleration and deceleration performance of a gas turbine in start up and shut down modes, respectively depends on the shaft inertia. In addition, the fastest the start up [60] and shut downs are, the greater the economic benefit and the life cycle reduction are going to be. Therefore start up and shut down processes should be optimized by taking into consideration several operational constraints. The gas turbine of the hybrid plant in this Case Study is exhibiting fast response behavior which is beneficial for the wind turbines.

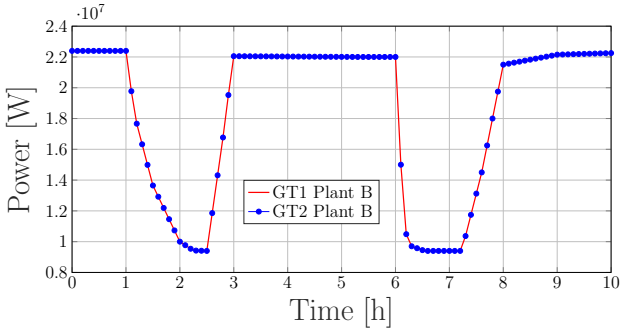

Figure 38: The variation of the power output from the gas turbines of Plant B expressed with respect to time.

Plant's A gas turbine will be inactive for almost 1 hour until it ramps up again and operate in a power setting close to its maximum, for the remaining 2 hours of operation. Meanwhile, the wind turbines remain operational during the entire 10 hours. Given that the power demanded from the plant has two occasions with significant load fluctuations, both of them have to be accommodated by the flexibility of the gas turbine since the wind farm's power capacity has a priority in the grid for this hybrid power plant.

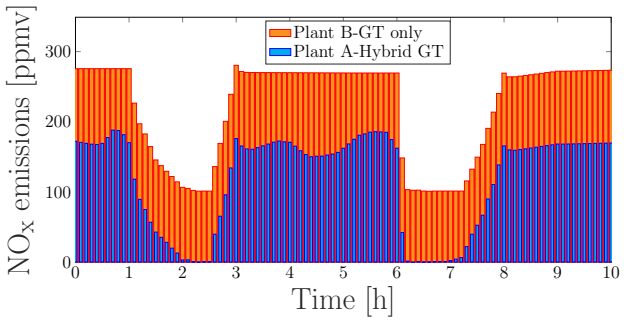

Figure 39: The variation of NO_x emissions for Plants A and B with respect to time.

For Plant B, both gas turbines have an identical load distribution and satisfy the fluctuating power demand effectively. In comparison to the gas turbine of Plant A, both gas turbines of Plant B operate at part load conditions and not at a power setting close to their design point. The power setting has a significant impact in the NO_x emissions of gas turbines, as observed from Eq. (5), since the higher the

pressure ratio, the higher the TET and therefore the higher the emissions are going to be.

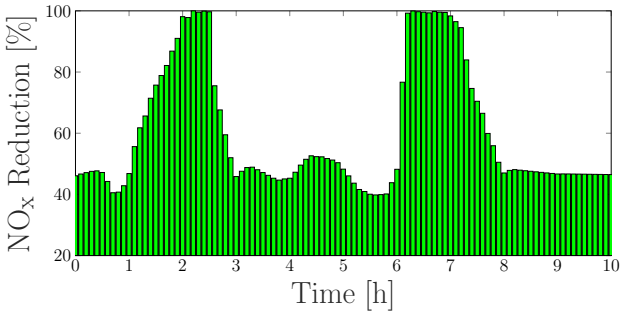

Figure 40: The variation of NO_x emissions percentage reduction of Plant A in comparison to Plant B with respect to time.

The NO_x emissions of both plants can be seen from Fig. 39. It is clear from Fig. 39, that the total NO_x emissions from both gas turbines of Plant B are significantly higher than the emissions of Plant A. However, if the gas turbines of Plant B were operating close to their design point conditions, and not at part load, the total emissions of Plant B would be higher. Nevertheless, the percentage of NO_x emissions reduction that can be achieved with Plant A in comparison to Plant B is significant, as it can be seen from Fig. 40.

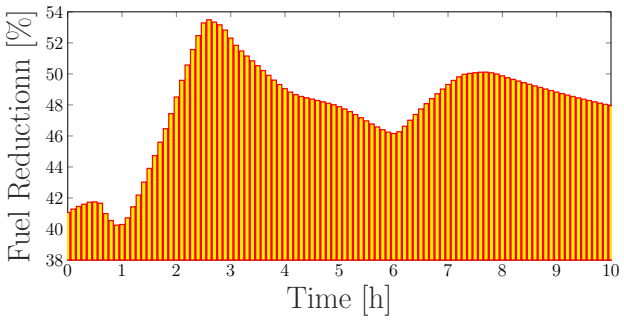

Figure 41: The accumulated variation of fuel percentage reduction of Plant A in comparison to Plant B with respect to time.

Specifically, the NO_x emissions of Plant A are initially 43% less than that of Plant B and increase to 100% when the gas turbine of Plant A shuts down. Between the two shut downs Plant's A NO_x emissions reduction varies from 40% to 50%. As far as the fuel consumption is concerned, Plant A demonstrates a potential to reduce the fuel consumption, in comparison to Plant B, by 48% as it can be seen from Fig. 41. Note that the fuel reduction represented in Fig. 41 refers to the accumulated fuel flow. This means that initially Plant A is consuming 41% less fuel than Plant B and after the entire 10 hour operation the total amount of fuel saved accounts to 48%. The transient gas turbine model provides the means for simulating harder operation profiles than the engine might normally experience in service in order to search for any potential operational issues. This Case Study highlights the importance of observations that arise from dynamic performance simulation of gas turbines, as these allow us to gain useful insights about their

behavior and optimize their operation according to their environmental impact and flexibility when working in partnership with renewables.

Finally, it should also be noted that if the portion of the renewables in a hybrid power plant is more than 70% with the wind speed conditions varying significantly with respect to time, then only one gas turbine might not suffice to fill the exhibited energy gap. A more flexible and environmentally friendlier configuration will be to operate two smaller gas turbine engines at part load settings instead of one larger gas turbine at base load. In such a case a pair of smaller gas turbines will be capable of accelerating and decelerating faster for meeting the fluctuating power demand while reducing their NO_x emissions. Fast transient maneuvers of the gas turbine are critical for maintaining the stability of the electricity grid from a hybrid gas/wind power plant. Additional promising technologies for wind speed forecasting might enable smoother transient gas turbine operation in a hybrid gas/wind power plant.

As far as practical issues are concerned the developed model can be further improved by a number of useful additions such as variable pitch control of the wind turbine [61, 54, 53], wind forecasting models [62], and adaptive model-tuning. Another important aspect of this developed model is the fact that it enables users to simulate numerous scenarios and can potentially feed its simulated measurements into a multi-objective optimization process for improving the performance of gas turbine. In addition, the model can accommodate degradation case studies [18] at component and system level for improving the prediction accuracy and the computational efficiency of diagnostic and prognostics algorithms.

4. Conclusions

In this paper, a dynamic gas turbine engine performance model is developed that aims to represent accurately the nonlinear behavior of flexible industrial gas turbines.

The gas turbine engine model is developed in MATLAB/Simulink environment. The engine model combines the iterative constant mass flow approach in steady state conditions for feeding several initial state parameters to the dynamic model, which implements the inter-component volume method.

By comparing the simulated measurements of a two-shaft industrial gas turbine engine model with data available from PROOSIS simulation package we observed the following:

- The developed engine model provides a fast and accurate performance assessment of a two-shaft industrial gas turbine.
- The observations of the engine model behavior corresponding to fast transients enabled the development of a controller for achieving smooth acceleration and deceleration.
- The maximum prediction errors between the Simulink model parameters and the PROOSIS ones is approximately 2%.

- The Simulink model converges almost 200 times faster than PROOSIS model, where for a 5 seconds transient maneuver with a time step of 1 millisecond its computation time is 0.24 seconds.

The dynamic response of the developed engine model has been also assessed for a hybrid gas/wind power plant consisting of 14 wind turbines. The outcome of this modeling scenario highlighted the fast transient maneuvers that the gas turbine experiences as the result of variable wind speeds and fluctuating power demand. Moreover, the hybrid power plant behavior emphasized the need for transient simulation studies since several operation challenges have to be addressed in order to optimize the energy dispatch as efficiently and flexibly as possible. Finally, the performance comparison of the hybrid power plant to a twin gas turbine plant for a 10 hour operating scenario demonstrated that the NO_x emissions reduction varies from 40% to 100% depending on the power setting of the gas turbine.

The engine model is characterized by its modularity, robustness and fast computational time which is crucial for assessing the dynamic performance behavior of a gas turbine engine for numerous transient operating scenarios. In addition, it has the capability of facilitating the design of engine controllers and the development of optimization modules for hybrid power plants. The modular architecture of the developed model is beneficial for developing and testing controllers, emissions prediction tools and for establishing a benchmark for model-based diagnosis and prognosis solutions. The developed dynamic engine model has the potential to enable the gas turbine users to optimize the operation of gas turbines in order to increase their availability and reduce their life cycle costs.

References

[1] L. Barelli, G. Bidini, A. Ottaviano, Integration of sofc/gt hybrid systems in micro-grids, Energy 118 (2017) 716–728.

[2] A. di Gaeta, F. Reale, F. Chiariello, P. Massoli, A dynamic model of a 100 kw micro gas turbine fuelled with natural gas and hydrogen blends and its application in a hybrid energy grid, Energy 129 (2017) 299–320.

[3] A. Mehrpanahi, G. Payganeh, M. Arbabtafti, Dynamic modeling of an industrial gas turbine in loading and unloading conditions using a gray box method, Energy 120 (2017) 1012–1024.

[4] L. Barelli, G. Bidini, A. Ottaviano, Part load operation of a sofc/gt hybrid system: Dynamic analysis, Applied energy 110 (2013) 173–189.

[5] H. Bahlawan, M. Morini, M. Pinelli, P. R. Spina, M. Venturini, Development of reliable narx models of gas turbine cold, warm and hot start-up, in: ASME Turbo Expo 2017: Turbomachinery Technical Conference and Exposition, American Society of Mechanical Engineers, 2017, pp. V009T27A007–V009T27A007.

[6] M. Tahan, E. Tsoutsanis, M. Muhammad, Z. A. Karim, Performance-based health monitoring, diagnostics and prognostics for condition-based maintenance of gas turbines: A review, Applied Energy 198 (2017) 122–144.

[7] Ge predix platform, `https://www.ge.com/digital/predix/platform`, accessed: 2017-10-19.

[8] Apple and ge partner to bring predix industrial apps to iphone and ipad, `https://www.apple.com/newsroom/2017/10/apple-and-ge-partner-to-bring-predix-industrial-apps-to-iphone-and-ipad/`, accessed: 2017-10-19.

[9] S. Barsali, A. De Marco, R. Giglioli, G. Ludovici, A. Possenti, Dynamic modelling of biomass power plant using micro gas turbine, Renewable Energy 80 (2015) 806–818.

[10] C. V. Ponce, D. Sáez, C. Bordons, A. Núñez, Dynamic simulator and model predictive control of an integrated solar combined cycle plant, Energy 109 (2016) 974–986.

[11] F. Alobaid, N. Mertens, R. Starkloff, T. Lanz, C. Heinze, B. Epple, Progress in dynamic simulation of thermal power plants, Progress in Energy and Combustion Science 59 (2017) 79–162.

[12] G. Ablay, A modeling and control approach to advanced nuclear power plants with gas turbines, Energy Conversion and Management 76 (2013) 899–909.

[13] S. Kang, K.-Y. Ahn, Dynamic modeling of solid oxide fuel cell and engine hybrid system for distributed power generation, Applied Energy 195 (2017) 1086–1099.

[14] Y. Cao, Y. Dai, Comparative analysis on off-design performance of a gas turbine and orc combined cycle under different operation approaches, Energy Conversion and Management 135 (2017) 84–100.

[15] E. Tsoutsanis, N. Meskin, M. Benammar, K. Khorasani, A component map tuning method for performance prediction and diagnostics of gas turbine compressors, Applied Energy 135 (2014) 572–585.

[16] M. Amozegar, K. Khorasani, An ensemble of dynamic neural network identifiers for fault detection and isolation of gas turbine engines, Neural Networks 76 (2016) 106–121.

[17] G. F. Ceschini, M. Venturini, T. Hubauer, A. Murarasu, et al., Optimization of statistical methodologies for anomaly detection in gas turbine dynamic time series, Journal of Engineering for Gas Turbines and Power 140 (3) (2018) 032401–10.

[18] E. Tsoutsanis, N. Meskin, M. Benammar, K. Khorasani, A dynamic prognosis scheme for flexible operation of gas turbines, Applied Energy 164 (2016) 686–701.

[19] E. Tsoutsanis, N. Meskin, Derivative-driven window-based regression method for gas turbine performance prognostics, Energy 128 (2017) 302–311.

[20] A. Stamatis, K. Mathioudakis, K. Papailiou, Adaptive simulation of gas turbine performance, Journal of Engineering for Gas Turbines and Power 112 (2) (1990) 168–175.

[21] Y. Yu, L. Chen, F. Sun, C. Wu, Neural-network based analysis and prediction of a compressor's characteristic performance map, Applied Energy 81 (1) (2007) 48–55.

[22] S.-K. Kim, P. Pilidis, J. Yin, Gas turbine dynamic simulation using simulink®, Tech. rep., SAE Technical Paper (2000).

[23] G. Crosa, F. Pittaluga, A. T. Martinengo, F. Beltrami, A. Torelli, F. Traverso, Heavy-duty gas turbine plant aerothermodynamic simulation using simulink, in: ASME 1996 Turbo Asia Conference, American Society of Mechanical Engineers, 1996, pp. V001T03A004–V001T03A004.

[24] J. Kim, T. Song, T. Kim, S. Ro, Model development and simulation of transient behavior of heavy duty gas turbines, Journal of Engineering for Gas Turbines and Power(Transactions of the ASME) 123 (3) (2001) 589–594.

[25] S. Camporeale, B. Fortunato, M. Mastrovito, A modular code for real time dynamic simulation of gas turbines in simulink, Journal of Engineering for Gas Turbines and Power 128 (3) (2006) 506–517.

[26] S. Bracco, F. Delfino, A mathematical model for the dynamic simulation of low size cogeneration gas turbines within smart microgrids, Energy 119 (2017) 710–723.

[27] A. Fawke, H. Saravanamuttoo, M. Holmes, Experimental verification of a digital computer simulation method for predicting gas turbine dynamic behaviour, Proceedings of the Institution of Mechanical Engineers 186 (1) (1972) 323–329.

[28] W. I. Rowen, Simplified mathematical representations of heavy-duty gas turbines, Journal of Engineering for Power 105 (4) (1983) 865–869.

[29] G. Crosa, G. Ferrari, A. Trucco, Modelling and recoupling the control loops in a heavy-duty gas turbine plant, ASME paper (1995) V005T15A002.

[30] C. Kong, J. Ki, K. Koh, Steady-state and transient performance simulation of a turboshaft engine with free power turbine, in: ASME 1999 International Gas Turbine and Aeroengine Congress and Exhibition, American Society of Mechanical

Engineers, 1999, p. V002T04A016.

[31] B. MacIsaak, H. Saravanamutto, A comparison of analog, digital and hybrid computing techniques for simulation of gas turbine performance, ASME Paper (74-GT) (1974) 127.

[32] N. Rahman, J. F. Whidborne, A numerical investigation into the effect of engine bleed on performance of a single-spool turbojet engine, Proceedings of the Institution of Mechanical Engineers, Part G: Journal of Aerospace Engineering 222 (7) (2008) 939–949.

[33] A. Alexiou, I. Roumeliotis, N. Aretakis, A. Tsalavoutas, K. Mathioudakis, Modeling contra-rotating turbomachinery components for engine performance simulations: the geared turbofan with contra-rotating core case, Journal of Engineering for Gas Turbines and Power 134 (11) (2012) 111701.

[34] N. U. Rahman, J. F. Whidborne, Real-time transient three spool turbofan engine simulation: a hybrid approach, Journal of Engineering for Gas Turbines and Power 131 (5) (2009) 051602.

[35] C. Wang, Y. Li, B. Yang, Transient performance simulation of aircraft engine integrated with fuel and control systems, Applied Thermal Engineering 114 (2017) 1029–1037.

[36] P. Pilidis, Digital simulation of gas turbine performance, Ph.D. thesis, University of Glasgow (1983).

[37] A. Benato, S. Bracco, A. Stoppato, A. Mirandola, Dynamic simulation of combined cycle power plant cycling in the electricity market, Energy Conversion and Management 107 (2016) 76–85.

[38] A. Benato, A. Stoppato, S. Bracco, Combined cycle power plants: A comparison between two different dynamic models to evaluate transient behaviour and residual life, Energy Conversion and Management 87 (2014) 1269–1280.

[39] A. Benato, S. Bracco, A. Stoppato, A. Mirandola, Lte: A procedure to predict power plants dynamic behaviour and components lifetime reduction during transient operation, Applied Energy 162 (2016) 880–891.

[40] P. P. Walsh, P. Fletcher, Gas turbine performance, John Wiley & Sons, 2004.

[41] H. I. H. Saravanamuttoo, G. F. C. Rogers, H. Cohen, Gas turbine theory, Pearson Education, 2001.

[42] B. MacIsaac, R. Langton, Gas turbine propulsion systems, Vol. 49, John Wiley & Sons, 2011.

[43] PROOSIS, Propulsion Object-Oriented Simulation Software, see also `http://www.proosis.com/` (2016).

[44] T. S. Pires, M. E. Cruz, M. J. Colaço, M. A. Alves, Application of nonlinear multivariable model predictive control to transient operation of a gas turbine and nox emissions reduction, Energy 149 (2018) 341–353.

[45] S. Taamallah, K. Vogiatzaki, F. Alzahrani, E. Mokheimer, M. Habib, A. Ghoniem, Fuel flexibility, stability and emissions in premixed hydrogen-rich gas turbine combustion: Technology, fundamentals, and numerical simulations, Applied energy 154 (2015) 1020–1047.

[46] N. Røkke, J. Hustad, S. Berg, Pollutant emissions from gas fired turbine engines in offshore practice: Measurements and scaling, in: ASME 1993 International Gas Turbine and Aeroengine Congress and Exposition, American Society of Mechanical Engineers, 1993, pp. V03AT15A021–V03AT15A021.

[47] S. Ouchen, A. Betka, J.-P. Gaubert, S. Abdeddaim, Simulation and real time implementation of predictive direct power control for three phase shunt active power filter using robust phase-locked loop, Simulation Modelling Practice and Theory 78 (Supplement C) (2017) 1 – 17.

[48] C. Shen, Y.-L. He, Y.-W. Liu, W.-Q. Tao, Modelling and simulation of solar radiation data processing with simulink, Simulation Modelling Practice and Theory 16 (7) (2008) 721 – 735.

[49] C. Kalathakis, N. Aretakis, I. Roumeliotis, A. Alexiou, K. Mathioudakis, Concentrated solar power components toolbox in an object oriented environment, Simulation Modelling Practice and Theory 70 (2017) 21–35.

[50] MATLAB, version 9.1 (R2016b), The MathWorks Inc., Natick, Massachusetts, 2016.

[51] S. Heier, Grid integration of wind energy: onshore and offshore conversion systems, John Wiley & Sons, 2014.

[52] E. Alizadeh, N. Meskin, K. Khorasani, A dendritic cell immune system inspired scheme for sensor fault detection and isolation of wind turbines, IEEE Transactions on Industrial Informatics PP (99) (2017) 1–1. `doi:10.1109/TII.2017.`

2746761.

[53] R. Gao, Z. Gao, Pitch control for wind turbine systems using optimization, estimation and compensation, Renewable Energy 91 (2016) 501–515.

[54] A. Rezaeiha, I. Kalkman, B. Blocken, Effect of pitch angle on power performance and aerodynamics of a vertical axis wind turbine, Applied Energy 197 (2017) 132–150.

[55] W. La Cava, K. Danai, L. Spector, P. Fleming, A. Wright, M. Lackner, Automatic identification of wind turbine models using evolutionary multiobjective optimization, Renewable Energy 87 (2016) 892–902.

[56] E. Tsoutsanis, N. Meskin, M. Benammar, K. Khorasani, Transient gas turbine performance diagnostics through nonlinear adaptation of compressor and turbine maps, Journal of Engineering for Gas Turbines and Power 137 (9) (2015) 091201–091201–12.

[57] E. Tsoutsanis, Y.-G. Li, P. Pilidis, M. Newby, Non-linear model calibration for off-design performance prediction of gas turbines with experimental data, The Aeronautical Journal 121 (1245) (2017) 1758–1777.

[58] A. Wan, F. Gu, J. Jin, X. Gu, Y. Ji, Modeling and optimization of shutdown process of combined cycle gas turbine under limited residual natural gas, Applied Thermal Engineering 101 (2016) 337–349.

[59] A. Buttler, F. Dinkel, S. Franz, H. Spliethoff, Variability of wind and solar power–an assessment of the current situation in the european union based on the year 2014, Energy 106 (2016) 147–161.

[60] M. Angerer, S. Kahlert, H. Spliethoff, Transient simulation and fatigue evaluation of fast gas turbine startups and shutdowns in a combined cycle plant with an innovative thermal buffer storage, Energy 130 (2017) 246–257.

[61] E. Muljadi, C. P. Butterfield, Pitch-controlled variable-speed wind turbine generation, IEEE Transactions on Industry Applications 37 (1) (2001) 240–246.

[62] W. Y. Cheng, Y. Liu, A. J. Bourgeois, Y. Wu, S. E. Haupt, Short-term wind forecast of a data assimilation/weather forecasting system with wind turbine anemometer measurement assimilation, Renewable Energy 107 (2017) 340–351.